Dynamical origin for winner-take-all competition in a biological network of the hippocampal dentate gyrus

Sang-Yoon Kim* and Woochang Lim†
Institute for Computational Neuroscience and Department of Science Education, Daegu National University of Education, Daegu 42411, Korea

(Received 17 August 2021; accepted 13 January 2022; published 28 January 2022)

We consider a biological network of the hippocampal dentate gyrus (DG). Computational models suggest that the DG would be a preprocessor for pattern separation (i.e., a process transforming a set of similar input patterns into distinct nonoverlapping output patterns) which could facilitate pattern storage and retrieval in the CA3 area of the hippocampus. The main encoding cells in the DG are the granule cells (GCs) which receive the input from the entorhinal cortex (EC) and send their output to the CA3. We note that the activation degree of GCs is very low ($\sim$5%). This sparsity has been thought to enhance the pattern separation. We investigate the dynamical origin for winner-take-all (WTA) competition which leads to sparse activation of the GCs. The whole GCs are grouped into lamellar clusters. In each cluster, there is one inhibitory (I) basket cell (BC) along with excitatory (E) GCs. There are three kinds of external inputs into the GCs: the direct excitatory EC input; the indirect feedforward inhibitory EC input, mediated by the HIPP (hilar perforant path-associated) cells; and the excitatory input from the hilar mossy cells (MCs). The firing activities of the GCs are determined via competition between the external E and I inputs. The E-I conductance ratio $\mathcal{R}_{\mathrm{E-I}}^{(\mathrm{con})*}$ (given by the time average of the ratio of the external E to I conductances) may represent well the degree of such external E-I input competition. It is thus found that GCs become active when their $\mathcal{R}_{\mathrm{E-I}}^{(\mathrm{con})*}$ is larger than a threshold $\mathcal{R}_{\mathrm{th}}^{*}$, and then the mean firing rates of the active GCs are strongly correlated with $\mathcal{R}_{\mathrm{E-I}}^{(\mathrm{con})*}$. In each cluster, the feedback inhibition from the BC may select the winner GCs. GCs with larger $\mathcal{R}_{\mathrm{E-I}}^{(\mathrm{con})*}$ than the threshold $\mathcal{R}_{\mathrm{th}}^{*}$ survive, and they become winners; all the other GCs with smaller $\mathcal{R}_{\mathrm{E-I}}^{(\mathrm{con})*}$ become silent. In this way, WTA competition occurs via competition between the firing activity of the GCs and the feedback inhibition from the BC in each cluster. Finally, we also study the effects of MC death and adult-born immature GCs on the WTA competition.

DOI: 10.1103/PhysRevE.105.014418

I. INTRODUCTION

The hippocampus, consisting of the dentate gyrus (DG) and the areas CA3 and CA1, is known to play a key role in memory formation, storage, and retrieval (e.g., episodic and spatial memory) [1,2]. In this hippocampus, the area CA3 has been often considered to operate as an autoassociation network, because there are extensive recurrent collateral synapses between the pyramidal cells in the CA3. The autoassociation network would store input "patterns" in modifiable synapses between the pyramidal cells. Then, when a partial or noisy version of the stored pattern is presented, activity of pyramidal cells would propagate along the previously strengthened pathways and reinstate the complete stored pattern, which is called the process of pattern completion. The idea of hippocampal autoassociation network has originated in the work of Marr [3,4] and was elaborated later by many others [5–13].

Storage capacity of autoassociation memory corresponds to the number of distinct patterns that can be stored and recalled. It could be increased if the input patterns are sparse (i.e., there are only a few active elements in each pattern) and nonoverlapping (orthogonalized) [i.e., active elements in one pattern may be likely to be (inactive) silent elements in other patterns] [3–13]. This process of transforming a set of input patterns into sparser and orthogonalized patterns is called pattern separation.

The DG is the gateway to the hippocampus that receives inputs from the entorhinal cortex (EC) via the perforant paths (PPs). Many computational models in Refs. [3–19] suggest that the principal granule cells (GCs) in the DG would perform pattern separation on the input patterns coming from the EC by sparsifying and orthogonalizing them (i.e., the input patterns from the EC would become sparser and orthogonalized via pattern separation of the GCs) which could facilitate pattern storage and retrieval in the CA3. Then, the pattern-separated outputs are projected (from the GCs) to the pyramidal cells in the CA3 via the mossy fibers (MFs). These sparse, but relatively strong MFs would play a role of "teaching inputs" (to the autoassociation network in the CA3) which could tend to trigger synaptic plasticity between the pyramidal cells and also between the pyramidal cells and the EC cells [11–13,15–17]. Thus, a new pattern could be stored in modified synapses (i.e., pattern storage could occur via synaptic plasticity caused by the MFs). In this way, pattern separation in the DG could facilitate pattern storage in the CA3.

In addition to the indirect inputs from the EC to the CA3 through the DG (i.e., the projections of the outputs from the

*sykim@icn.re.kr
†wclim@icn.re.kr

DG onto the CA3 via the MFs would be responsible for pattern storage), direct weaker inputs from the EC to the CA3 pyramidal cells via PPs represent partial or noisy version of patterns to be recalled. These direct EC inputs would activate a subset of pyramidal cells in the CA3 which would in turn activate other pyramidal cells through the previously strengthened synapses until the complete stored pattern is recalled (i.e., stored patterns would be recalled via pattern completion) [11–13,15–17]. In this way, the direct EC inputs to the CA3 would play a role of retrieval cue for recalling the previously stored patterns via pattern completion, in contrast to the indirect EC inputs via the MFs from the DG which could cause synaptic plasticity leading to pattern storage.

We also note that convergent evidences, attributing pattern separation to the DG, have been experimentally accumulated [20,21]. For example, electrophysiological recordings in GCs in the DG of the rodent [22] and human functional magnetic resonance imaging in the DG [23] have largely supported the pattern-separation ideas suggested in computational models. In addition, lesion studies in rats showed that DG-lesioned rats were impaired in pattern separation [24–27], which confirmed that the DG is necessary for pattern separation.

In this paper, we focus on the hippocampal DG, and consider a biological network of the DG. The principal GCs in the DG network receive the input patterns from the EC via the PPs, perform pattern separation on the EC inputs, and project their outputs onto the CA3 via MFs. In this process of pattern separation, the activation degree D_a of the GCs is so low ($D_a \sim 5$ %) [14]. The GCs exhibit sparse firing activity via competitive learning [6,11,13,14], and the sparsity has been considered to enhance the pattern separation [11–19].

Here, we investigate the dynamical origin of the winner-take-all (WTA) competition which leads to sparse activation of the GCs (improving the pattern separation) [28–37]. We first note that the whole GCs are grouped into the lamellar clusters [38–41]. In our DG network, there are 20 (nonoverlapping) clusters. Each cluster consists of 100 excitatory (E) GCs along with one inhibitory (I) basket cell (BC). Hence, the total number of BCs ($N_{\rm BC}$) is 20, corresponding to 1/100 of the total number of GCs ($N_{\rm GC} = 2,000$); the GC to BC ratio (100 : 1) is consistent with anatomical data [42–46]. Thus, the GCs and the BC in each cluster form an E-I dynamical loop where all the GCs are coupled to the single BC; there are no couplings between the GCs. Hence, all the GCs provide excitation to the BC which then gives back the feedback inhibition to all the GCs. Then, competition between the firing activity of the GCs and the feedback inhibition from the BC selects which GCs fire. Intuitively, strongly active GCs may survive under the feedback inhibition of the BC (i.e., they become winners), while weakly active GCs become silent in response to the feedback inhibition of the BC. Through intensive computational work for WTA competition, we get the quantitative dynamical origin for WTA, consistent with the intuitive thinking.

The firing activities of the GCs are determined via competition between the external E and I inputs to the GCs. The EC is the main external input source for the GCs. There are direct excitatory EC input via the PPs and indirect feedforward inhibitory EC input, mediated by the HIPP (hilar perforant path-associated) cells in the hilus of the DG [14–17,19] (e.g., see Fig. 1 in Ref. [14]); random connections for EC → GC and EC → HIPP cell → GC [see Fig. 1(b)].

In the DG, the hilus, consisting of the excitatory mossy cells (MCs) and the inhibitory HIPP cells, underlies the GC layer (composed of GCs and BCs) [14–19,47–53]. Here, lamellar cluster organization for the MCs is also considered, like the case of the GCs and the BCs [15–17]. In each cluster, there are 4 MCs; each MC receives excitatory inputs from all the GCs in the same cluster [i.e., lamellar connection in Fig. 1(b)]. However, each MC in a cluster makes excitatory projection randomly to the GCs and the BCs in other clusters [i.e., cross-lamellar connections in Fig. 1(b)] [15–17,52].

Thus, there are two types of excitatory cells (i.e., GCs and MCs) in the DG rather than one kind of pyramidal cells in the CA3 and the CA1. The MCs in a cluster controls the firing activity of the GC-BC loop in other clusters via cross-lamellar connections by providing excitation to both the GCs and the BCs. Thus, there appears a third type of excitatory input from the hilar MCs into the GCs, in addition to the two kinds of external EC inputs (i.e., the direct excitatory EC input and the indirect feedforward inhibitory EC input, mediated by the HIPP cells). Consequently, there are three kinds of external inputs into the GCs; two types of excitatory inputs from the EC via PPs and from the MCs and one kind of inhibitory input from the HIPP cells.

For characterization of the degree of the external E-I input competition, we introduce the E-I conductance ratio $\mathcal{R}_{\rm E-I}^{({\rm con})*}$, given by the time average of the ratio of the external E to I conductances, $\overline{g_{\rm E}(t)/g_{\rm I}(t)}$ (the overline denotes time average); the excitatory conductance $g_{\rm E}(t) = g_{\rm EC}(t) + g_{\rm MC}(t)$ [$g_{\rm EC}(t)$: conductance of the excitatory EC input and $g_{\rm MC}(t)$: conductance of the excitatory MC input] and the inhibitory conductance $g_{\rm I}(t) = g_{\rm HIPP}(t)$ (conductance of the inhibitory HIPP input). When their $\mathcal{R}_{\rm E-I}^{({\rm con})*}$ is greater than a threshold $\mathcal{R}_{th}^*$, GCs become active; otherwise, they become silent. The mean firing rates (MFRs) of the active GCs are also found to be strongly correlated with $\mathcal{R}_{\rm E-I}^{({\rm con})*}$ (i.e., with increasing $\mathcal{R}_{\rm E-I}^{({\rm con})*}$, their MFRs also increase linearly). In this way, the degree of the firing activity of the GCs may be well characterized in terms of their $\mathcal{R}_{\rm E-I}^{({\rm con})*}$.

Then, the feedback inhibition from the BC selects the winner GCs in each cluster. GCs with larger $\mathcal{R}_{\rm E-I}^{({\rm con})*}$ than the threshold $\mathcal{R}_{th}^*$ are found to survive under the feedback inhibition, and they become winners, while all the other GCs with smaller $\mathcal{R}_{\rm E-I}^{({\rm con})*}$ become silent in response to the feedback inhibition. Thus, WTA competition occurs through competition between the firing activity of the GCs and the feedback inhibition from the BC.

During epileptogenesis MF sprouting and hilar cell (MC and HIPP cell) death occur [54,55]. Here, we are concerned about the MC loss. In contrast to MC death, young immature GCs (imGCs) appear via adult neurogenesis [16,56–61]. Finally, we also study the effects of MC death and adult-born imGCs on the WTA competition.

This paper is organized as follows. In Sec. II, we describe a biological network of the hippocampal DG. Then, in the main Sec. III, we investigate dynamical origin for the WTA competition and effects of MC death and adult-born imGCs on the

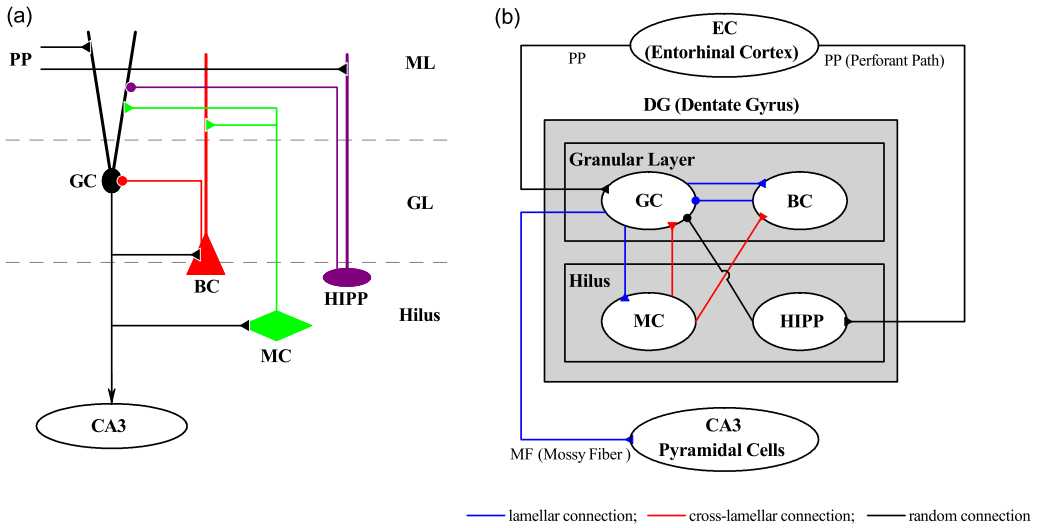

FIG. 1. Hippocampal dentate gyrus (DG) spiking neural network. (a) Schematic representation of major cells and synaptic connections included in our DG network. The DG consists of the granule layer (GL), the hilus, and the molecular layer (ML). GC, BC, MC, and HIPP represent granule cell, basket cell, mossy cell, and hilar perforant-path associated cell, respectively. Dendrites are denoted by thick lines. External input from the entorhinal cortex (EC) is provided via perforant path (PP). Lines with triangles and circles denote excitatory and inhibitory synapses, respectively. (b) Box diagram for our DG network with three types of synaptic connections. Blue, red, and black lines represent lamellar, cross-lamellar, and random connections, respectively.

WTA competition. Finally, we give summary and discussion in Sec. IV.

II. BIOLOGICAL NETWORK OF THE HIPPOCAMPAL DENTATE GYRUS

In this section, we describe our biological network of the hippocampal DG, and briefly present the governing equations for the population dynamics; for details, refer to Appendices A and B. Hyperexcitability of the GCs via sprouting of the MFs has been studied in biological networks of the DG with a high degree of anatomical and physiological realism [54,55]. These realistic biological networks consist of the hilar cells (e.g., MCs and HIPP cells) as well as the GCs, in contrast to the prior abstract computational models which focused primarily on the GCs (without considering the hilar cells) and performed pattern separation and completion [3–13]. However, the above works in the biological networks did not address specifically the pattern separation, although hyperexcitability of the GCs would decrease sparsity of the GC activity, leading to increase in overlap and then to decrease in pattern separation.

To bridge the gap between the abstract computational models and the realistic biological networks, a relatively small-scale simplified network, based on the prior ideas of the abstract models and including not only the GCs, but also the hilar cells, was developed to investigate the pattern separation [14,15]. Recently, the effects of hilar ectopic GCs, hyperexcitability, and GC dendrites on the pattern separation have also been investigated in the biological spiking neural networks [16–19].

Here, we develop a spiking neural network for the hippocampal DG, based on the anatomical and the physiological properties described in Refs. [14,15,19]. Obviously, our spiking neural network will not capture all the detailed anatomical and physiological complexity of the DG. However, with limited, but key elements and synaptic connections in our DG network, dynamical origin for the WTA could be successfully studied. Hence, our DG network model would build a foundation upon which additional complexity can be added and guide further research.

A. Architecture of the spiking neural network of hippocampal dentate gyrus

Figure 1(a) shows schematic representation of major cells and synaptic connections included in our hippocampal DG network and Fig. 1(b) shows the box diagram for our DG network with three types of lamellar (blue), cross-lamellar (red), and random (black) synaptic connections. In the DG, we consider the granular layer (GL), consisting of the excitatory GCs and the inhibitory BCs, the underlying hilus, composed of the excitatory MCs and the inhibitory HIPP cells, and the upper molecular layer (ML). We note that there are two types of excitatory cells, GCs and MCs, in contrast to the case of the CA3 and CA1 with only one type of excitatory pyramidal cells.

From the outside of the DG, the EC provides the external excitatory inputs randomly to the GCs and the HIPP cells (that provide inhibition to the GCs) via PPs [14–17,19], as shown in Fig. 1 in Ref. [14]. The HIPP cells have dendrites extending to the outer ML, where they are targeted by the PPs, along with axons projecting to the outer ML (primarily to the GCs) [14,62–66].

Thus, the GCs receive direct excitatory EC input via PPs (EC → GC) and indirect feedforward inhibitory EC input, mediated by the hilar HIPP cells (EC → HIPP → GC). The GCs are grouped into lamellar clusters [38–41], and one inhibitory BC exists in each cluster [14]. Thus, a dynamical GC-BC loop is formed, and the BC (receiving the excitation

from all the GCs) provides the feedback inhibition to all the GCs [i.e., lamellar connection in Fig. 1(b)]. In a cluster, there are no synaptic couplings between the GCs. Also, there are no intercluster interactions for the GCs and the BCs.

We also consider lamellar organization for the hilar MCs [15–17,52] (i.e., all the MCs also are grouped into lamellar clusters). Each MC in a cluster receives excitation from all the GCs in the same cluster (lamellar connection), while it makes excitatory projection randomly to GCs and BCs in other clusters with the probability 20% [cross-lamellar connection in Fig. 1(b)] [52]. These MCs control the activity of the GC-BC loop in each cluster via cross-lamellar connections by providing excitation to the GCs and the BC.

Thus, the GCs receive the direct excitatory MC input (MC $\rightarrow$ GC) and the indirect disynaptic inhibitory MC input, mediated by the BC (MC $\rightarrow$ BC $\rightarrow$ GC). In this way, from the outside of the cluster, the GCs receive two types of excitatory inputs from the EC and the MCs and one kind of inhibitory input from the HIPP cells, and within the cluster they receive the feedback inhibition from the BC (receiving the excitation from the GCs and the MCs).

We develop a one-dimensional ring network for the hippocampal DG. Due to the ring structure, the network has advantage for computational efficiency, and its visual representation may also be easily made. Based on the anatomical data given in Refs. [14,15,19], we choose the numbers of the constituent cells (GCs, BCs, MCs, and HIPP cells) and the EC cells in our DG network and the connection probabilities between them.

Here, we consider a scaled-down spiking neural network where the total number of excitatory GCs is $N_{\rm GC}$ (=2000), corresponding to $\frac{1}{500}$ of the 10^6 GCs found in rats [67]. These GCs are grouped into the N_c (=20) lamellar clusters [38–41]. Then, in each cluster, there exist $n_{\rm GC}^{(c)}$ (=100) GCs and one inhibitory BC [15–17,55]. Thus, the number of BCs in the whole DG network becomes $N_{\rm BC}$ (=20), corresponding to 1/100 of $N_{\rm GC}$; the GC to BC ratio (100 : 1) is consistent with anatomical data [42–46]. In this way, in each cluster, a dynamical GC-BC loop is formed, and the BC (receiving the excitation from all the GCs) provides the feedback inhibition to all the GCs via lamellar connections.

In addition to the GCs and the BCs in the GL, the hilus consists of the excitatory MCs and the inhibitory HIPP cells. In rats, the number of MCs, $N_{\rm MC}$, varies from 30 000 to 50 000, which correspond to 3–5 MCs per 100 GCs [43,67]. Hence, we choose $N_{\rm MC} = 80$ in our DG network. Also, the estimated number of HIPP cells, $N_{\rm HIPP}$, is about 12 000 in rats [43], corresponding to about 2 HIPP cells per 100 GCs. In our DG network, the number of the HIPP cells is chosen as $N_{\rm HIPP} = 40$.

We also consider lamellar organization for the MCs, as in Refs. [15–17,52]; for simplicity, lamellar organization for the HIPP cells is not considered [15]. Like the case of the GCs and the BCs, the whole MCs ($N_{\rm MC} = 80$) are grouped into the 20 lamellar clusters. Hence, in each cluster, there are four MCs. Each MC in a cluster receives excitation from all the GCs in the same cluster via lamellar connections, while it provides excitation randomly to the GCs and the BCs in other clusters via cross-lamellar connections with the connection probability $p^{\rm (GC,MC)}$ ($p^{\rm (BC,MC)}$) = 20% [52]. In this way, the MCs control the activity of the GC-BC loop in each cluster by providing excitation to the GCs and the BC through cross-lamellar connections.

The EC layer II is the external source providing the excitatory inputs randomly to the GCs and the HIPP cells via the PPs [14,19]. The estimated number of the EC layer II cells, $N_{\rm EC}$, is about 200 000 in rats, which corresponds to 20 EC cells per 100 GCs [68]. Hence, $N_{\rm EC} = 400$ in our network. The activation degree D_a of the EC cells is chosen as 10% [69]. We randomly choose 40 active ones among the 400 EC (layer II) cells. Each active EC cell is modeled in terms of the Poisson spike train with frequency of 40 Hz [70]. Here, the random-connection probability $p^{\rm (GC,EC)}$ ($p^{\rm (HIPP,EC)}$) from the presynaptic EC cells to a postsynaptic GC (HIPP cell) is 20% [14,19]. Hence, each GC or HIPP cell is randomly connected with the average number of 80 EC cells (among which the average number of active EC cells is just 8).

Each GC in the cluster receives inhibition from the randomly connected HIPP cells with the connection probability $p^{\rm (GC,HIPP)} = 20\,\%$ [14,19]. Then, the firing activity of the GCs is determined via competition between the two types of excitatory inputs from the EC cells and from the MCs and the inhibitory input from the HIPP cells. Eventually, winner GCs in each cluster are selected through competition between the firing activity of the GCs and the feedback inhibition from the BC; strongly active GCs may survive under the feedback inhibition from the BC.

B. Single neuron models and synaptic currents in the DG spiking neural network

As elements of the hippocampal DG spiking neural network, we choose leaky integrate-and-fire (LIF) spiking neuron models with additional afterhyperpolarization (AHP) currents, determining refractory periods, as in our prior study of cerebellar ring network [71,72]. This LIF spiking neuron model is one of the simplest spiking neuron models [73]. Because of its simplicity, it can be easily analyzed and simulated. Hence, it has been very popularly used as a spiking neuron model.

Our DG network is composed of four populations of GCs, BCs, MCs, and HIPP cells. The state of a neuron in each population is characterized by its membrane potential. Then, time evolution of the membrane potential is governed by four types of currents into the neuron; the leakage current, the AHP current, the external constant current, and the synaptic current.

We note that the equation for a single LIF neuron model (without the AHP current and the synaptic current) describes a simple parallel resistor-capacitor (RC) circuit. Here, the first type of leakage current is due to the resistor and the integration of the external current is due to the capacitor which is in parallel to the resistor. When its membrane potential reaches a threshold, a neuron fires a spike, and then the second type of AHP current follows. As the decay time of the AHP current is increased, the refractory period becomes longer. Here, we consider a subthreshold case where the third type of external constant current is zero [19].

Detailed explanations on the leakage current and the AHP current, associated with each type of single neuron (GC, BC, MC, and HIPP cell), are presented in Appendix A. The

parameter values for the capacitance, the leakage current, and the AHP current for the GC, BC, MC, and HIPP cell are shown in Table I in Appendix A. These values are based on physiological properties of the GC, BC, MC, and HIPP cell [19,49].

Next, we consider the fourth type of synaptic current. Detailed explanations on the synaptic current are given in Appendix B; here, we present just a brief and clear explanation on it. There are three kinds of synaptic currents from a presynaptic source population to a postsynaptic neuron in the target population, two kinds of excitatory AMPA and NMDA receptor-mediated synaptic currents, and one type of inhibitory GABA receptor-mediated synaptic current. In each R (AMPA, NMDA, and GABA) receptor-mediated synaptic current, the synaptic conductance is given by the product of the synaptic strength per synapse, the average number of afferent synapses (connected to a postsynaptic neuron), and the fraction of open ion channels.

The postsynaptic ion channels are opened due to the binding of neurotransmitters (emitted from the source population) to receptors in the target population. The time course of the fraction of open ion channels is given by a sum of "double-exponential" functions over presynaptic spikes. The double-exponential function, corresponding to contribution of a presynaptic spike, is controlled by the synaptic rising time constant, the synaptic decay time constant, and the synaptic latency time constant; for details, refer to Eq. (B4) in Appendix B.

As in our prior works in the cerebellum [71,72], the fraction of open ion channels (i.e., contributions of summed effects of presynaptic spikes) may be well approximated by the bin-averaged spike rate of presynaptic neurons. Then, the synaptic conductance may be approximately obtained in terms of the product of the synaptic strength per synapse, the average number of afferent synapses, and the bin-averaged spike rate of presynaptic neurons.

The parameter values for the synaptic strength per synapse, the synaptic rising time constant, the synaptic decay time constant, the synaptic latency time constant, and the synaptic reversal potential for the synaptic currents into the GCs and for the synaptic currents into the HIPP cell, the MC, and the BC are given in Tables II and III, respectively, in Appendix B. These parameter values are also based on the physiological properties of the relevant cells [19,74–81].

All of our source codes for computational works were written in C programming language. Numerical integration of the governing equation for the time evolution of states of individual spiking neurons is done by employing the second-order Runge-Kutta method with the time step 0.1 ms. We will release our source codes at the public databases such as ModelDB.

III. DYNAMICAL ORIGIN FOR THE WINNER-TAKE-ALL COMPETITION

As a preprocessor for the CA3, the GCs in the DG would perform the pattern separation, facilitating the pattern storage and completion in the CA3. The GCs exhibit sparse firing activity through competitive learning, which has been thought to improve the pattern separation. In this section, we investigate the dynamical origin of the WTA competition, leading to the sparse activation of the GCs. The firing activity of the GCs may be well determined in terms of the E-I conductance ratio $\mathcal{R}_{\rm E-I}^{(\rm con)*}$ (given by the time average of the ratio of the external E to I conductances). GCs become active (i.e., they become winners) only when their $\mathcal{R}_{\rm E-I}^{(\rm con)*}$ is larger than a threshold $\mathcal{R}_{th}^{*}$. WTA competition is thus found to occur via competition between the firing activity of the GCs and the feedback inhibition from the BC in each cluster. We also study the effects of the MC death and the adult-born imGCs on the WTA competition.

A. Firing activity of GCs in the presence of the external excitatory EC and the inhibitory HIPP inputs

In this subsection, we study firing activity of the GCs under the external excitatory input from the EC cells and the inhibitory input from the HIPP cells. The firing activity of the GCs is found to be determined via competition between the excitatory EC input and the inhibitory HIPP input. Particularly, such competition may be well represented in terms of the E-I synapse ratio $\mathcal{R}_{\rm E-I}^{(\rm syn)}$, given by the ratio of the number of the presynaptic EC cells ($M_{\rm syn}^{(\rm GC,EC)}$) to the number of the presynaptic HIPP cells ($M_{\rm syn}^{(\rm GC,HIPP)}$).

Figure 2 shows the external input from the EC. There are direct excitatory input from the EC cells and indirect feedforward inhibitory EC input, mediated by the hilar HIPP cells [see Fig. 1]. Among the 400 EC cells, randomly chosen 40 active cells make spikings (i.e., activation degree $D_a = 10\%$). Each active EC cell is modeled in terms of the Poisson spike train with frequency of 40 Hz. After a break stage ($t = 0$–300 ms), Poisson spike train of each active EC cell follows during the stimulus stage ($t = 300$–$30,300$ ms; the stimulus period T_s is 3×10^4 ms).

Population firing activity of the active EC cells may be well visualized in the raster plot of spikes in Fig. 2(a1) which is a collection of spike trains of individual active EC cells; for convenience, only a part from $t = 300$ to 1300 ms is shown in the raster plot of spikes. Spikes of the active EC cells are completely scattered without forming any synchronized "spiking stripes," and hence the population state of the active ECs becomes desynchronized. As a population quantity showing collective firing behaviors, we use an instantaneous population spike rate (IPSR) which may be obtained from the raster plots of spikes [82–87]; for details, refer to Appendix C. The IPSR $R_{\rm EC}(t)$ of the active EC cells is shown in Fig. 2(a2), and it shows relatively small noisy fluctuations around its time average (i.e., $\overline{R_{\rm EC}(t)} = 40$ Hz) without distinct synchronous oscillations.

The active EC cells provide direct excitatory input and indirect feedforward inhibitory input, mediated by the HIPP cells, to the GCs. Thus, the EC cells and the HIPP cells become the excitatory and the inhibitory input sources to the GCs, respectively. We note that each HIPP cell is randomly connected to the average number of 80 EC cells with the connection probability $p^{(\rm HIPP,EC)} = 20\%$, among which the average number of active EC cells is 8. Figures 2(b1) and 2(b2) show the raster plot of spikes of the active HIPP cells and the corresponding IPSR $R_{\rm HIPP}(t)$. Among the 40 HIPP

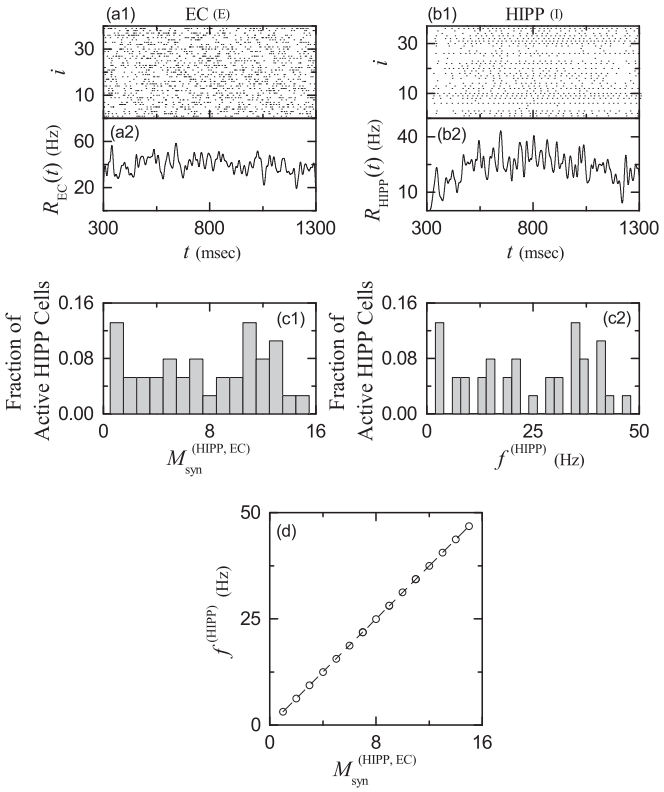

FIG. 2. External inputs from the EC. Direct excitatory (E) EC input via PP: (a1) Raster plot of spikes of 40 active EC cells. (a2) Instantaneous population spike rate $R_{\rm EC}(t)$ of active EC cells. Band width for $R_{\rm EC}(t)$: $h = 20$ ms. Indirect disynaptic inhibitory (I) EC input, mediated by the hilar HIPP cells: (b1) Raster plot of spikes of 37 active HIPP cells. (b2) Instantaneous population spike rate $R_{\rm HIPP}(t)$ of active HIPP cells. Band width for $R_{\rm HIPP}(t)$: $h = 20$ ms. (c1) Normalized histogram of $M_{\rm syn}^{\rm (HIPP,EC)}$ (number of presynaptic active EC cells onto the postsynaptic active HIPP cells). Bin size for the histogram is 1. (c2) Normalized histogram of $f^{\rm (HIPP)}$ [mean firing rate (MFR) of active HIPP cells]. Bin size for the histogram is 2 Hz. (d) Plot of $f^{\rm (HIPP)}$ versus $M_{\rm syn}^{\rm (HIPP,EC)}$.

cells, 37 HIPP cells are active, while the remaining 3 HIPP cells (without receiving excitatory input from the active EC cells) are silent; the activation degree of the HIPP cells is 92.5%. Also, the spiking of the active HIPP cells begins from $t \simeq 320$ ms [i.e. about 20 ms delay for the firing onset of the HIPP cells with respect to the firing onset ($t = 300$ ms) of the active EC cells].

As in the case of the active EC cells, no synchronized spiking stripes are shown in the raster plot of spikes of the active HIPP cells. However, unlike the case of the active EC cells (showing stochastic firing activity), the spike train of each active HIPP cell seems to be quasi-regular with its own MFR (i.e., each active HIPP cell seems to exhibit a quasi-regular firing activity). However, their MFRs seem to vary very differently depending on the active HIPP cells. Due to such diverse MFRs, no synchronized spiking stripes appear in the raster plot of spikes of the active HIPP cells. Hence, their IPSR $R_{\rm HIPP}(t)$ also shows noisy fluctuations around its time average (i.e., $\overline{R_{\rm HIPP}(t)} = 23$ Hz) without synchronous oscillations.

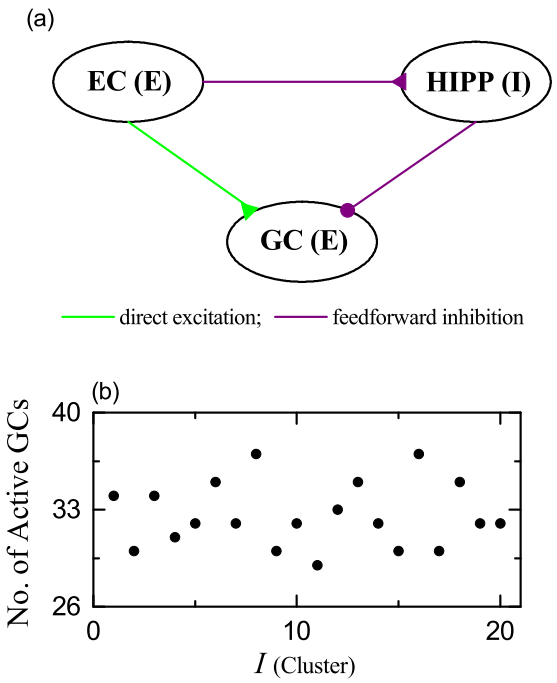

FIG. 3. Firing activity of GCs in the presence of only the external direct excitatory EC input and indirect feedforward inhibitory EC input, mediated by the HIPP cells. (a) Diagram for the external direct excitatory input from the EC cells (green line) and indirect feedforward inhibitory input from the EC cells, mediated by the HIPP cells (violet line) into the GCs. (b) Plot of number of active GCs versus I (cluster index).

In Figs. 2(c1) and 2(c2), we discuss how MFRs of the active HIPP cells become diverse. The number of presynaptic active EC cells $M_{\rm syn}^{\rm (HIPP,EC)}$ for the postsynaptic active HIPP cells is broadly distributed in Fig. 2(c1). Its range is [1, 15], the mean is 7.8, and the standard deviation from the mean is 4.5; three silent HIPP cells have no active presynaptic EC cells. The MFR $f^{\rm (HIPP)}$ of each active HIPP cell is obtained by dividing the total number of spikes by the stimulus period T_s ($=3 \times 10^4$ ms). Figure 2(c2) shows broad distribution of the MFRs. Its range is [2.6, 47.8] Hz, the population-averaged MFR $\langle f^{\rm (HIPP)} \rangle = 22.9$ Hz, and the standard deviation from $\langle f^{\rm (HIPP)} \rangle$ is 14.1 Hz. Because of these diverse MFRs, the active HIPP cells exhibit no collective synchronized firing activity. We also note that there exists a strong positive correlation (with the Pearson's correlation coefficient $r = 0.9999$) between $M_{\rm syn}^{\rm (HIPP,EC)}$ (number of presynaptic active EC cells) and $f^{\rm (HIPP)}$ (MFRs of the postsynaptic HIPP cells) [see Fig. 2(d)] [88]; the larger the number of presynaptic active EC cells, the higher the MFR of the (postsynaptic) active HIPP cell.

Then, we first investigate firing activity of GCs in the presence of only the external direct excitatory EC input and indirect feedforward inhibitory EC input, mediated by the HIPP cells. Figure 3(a) shows a diagram for the external direct excitatory input from the EC cells (green line) and indirect feedforward inhibitory inputs from the EC cells, mediated by the HIPP cells (violet line) into the GCs. In this case, the number of active GCs in each cluster ($I = 1, \ldots, 20$) is shown in Fig. 3(b). A GC with at least one spike during the stimulus

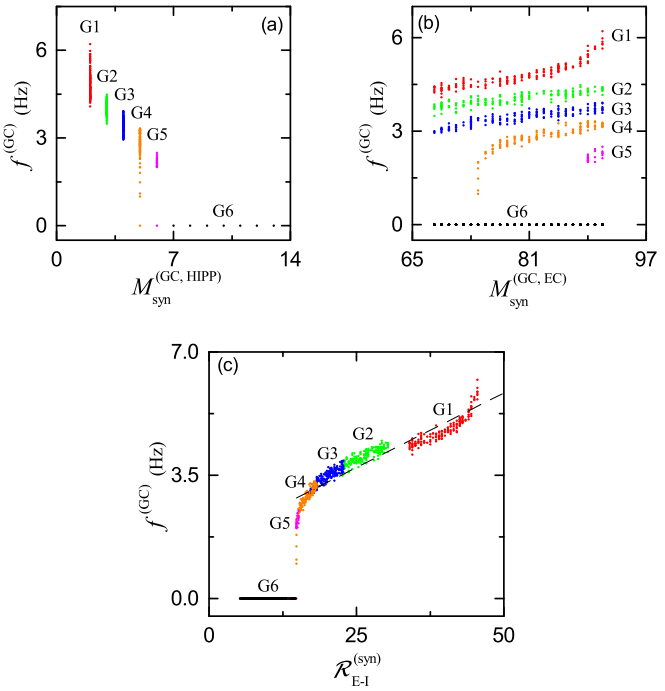

FIG. 4. Firing activity of GCs via competition between the numbers of presynaptic EC and HIPP cells. Plots of $f^{(GC)}$ (MFR of GCs) versus (a) $M_{syn}^{(GC,HIPP)}$ (number of presynaptic HIPP cells) and (b) $M_{syn}^{(GC,EC)}$ (number of presynaptic EC cells). GCs are decomposed into groups Gn ($n = 1, \ldots, 6$) with different number of presynaptic HIPP cells $M_{syn}^{(GC,HIPP)}$: G1 (red color online) [$M_{syn}^{(GC,HIPP)} = 2$], G2 (green) [$M_{syn}^{(GC,HIPP)} = 3$], G3 (blue) [$M_{syn}^{(GC,HIPP)} = 4$], G4 (orange) [$M_{syn}^{(GC,HIPP)} = 5$], G5 (violet) [$M_{syn}^{(GC,HIPP)} = 6$], and G6 (black) [$M_{syn}^{(GC,HIPP)} \geqslant 7$]. (c) Plot of $f^{(GC)}$ versus the E-I synapse ratio $\mathcal{R}_{E-I}^{(syn)}$ ($=M_{syn}^{(GC,EC)} / M_{syn}^{(GC,HIPP)}$); a fitted dashed line is given.

period T_s ($= 3 \times 10^4$ ms) is active; otherwise, silent. In this case, the total number of active GCs is 652, and hence the activation degree is $D_a = 32.6\%$. For the distribution of the number of active GCs in each cluster, its range is [29, 37], the mean is 32.6, and the standard deviation from the mean is 2.35.

In the case of Fig. 3(a), firing activity of the GCs is determined via competition between the direct excitatory EC input and the indirect feedforward inhibitory EC input, mediated by the HIPP Cells. The strength of direct excitatory EC input may be represented by the number of presynaptic EC cells, $M_{syn}^{(GC,EC)}$ and the strength of indirect inhibitory EC input, mediated by the HIPP cells, can also be denoted by the number of presynaptic HIPP cells, $M_{syn}^{(GC,HIPP)}$. Then, the E-I synapse ratio $\mathcal{R}_{E-I}^{(syn)}$, defined by

$$\mathcal{R}_{E-I}^{(syn)} = \frac{M_{syn}^{(GC,EC)}}{M_{syn}^{(GC,HIPP)}}, \tag{1}$$

represents well the competition between the excitatory input from the EC cells and the inhibitory input from the HIPP cells.

Figure 4(a) shows a plot of $f^{(GC)}$ (MFR of the GCs) versus $M_{syn}^{(GC,HIPP)}$ (number of the presynaptic HIPP cells). For the distribution of $M_{syn}^{(GC,HIPP)}$, its range is [2, 13], the mean is 7.9, and the standard deviation from the mean is 3.5. Depending on $M_{syn}^{(GC,HIPP)}$, the whole GCs are decomposed into the 6 groups Gn (n $= 1, \ldots, 6$) with different values of $M_{syn}^{(GC,HIPP)}$. In the group G1 (red color online) with $M_{syn}^{(GC,HIPP)} = 2$, G2 (green) with $M_{syn}^{(GC,HIPP)} = 3$, G3 (blue) with $M_{syn}^{(GC,HIPP)} = 4$, G4 (orange) with $M_{syn}^{(GC,HIPP)} = 5$, G5 (violet) with $M_{syn}^{(GC,HIPP)} = 6$, and G6 (black) with $M_{syn}^{(GC,HIPP)} \geqslant 7$, the number of GCs (fraction) is 156 (7.8%), 169 (8.45%), 173 (8.65%), 170 (8.50%), 152 (7.6%), and 1180 (59%), respectively. With increasing $M_{syn}^{(GC,HIPP)}$, $f^{(GC)}$ (MFRs of the GCs) tend to decrease due to increase in the inhibitory input from the HIPP cells. In the groups G1, G2, and G3, only active GCs appear. However, from the group G4, silent GCs also appear along with active GCs, and eventually in the group G6, all the GCs are silent.

Figure 4(b) shows a plot of $f^{(GC)}$ versus $M_{syn}^{(GC,EC)}$ (number of the presynaptic EC cells). For the distribution of $M_{syn}^{(GC,EC)}$, its range is [68, 91], the mean is 79.4, and the standard deviation from the mean is 6.8. In each Gn ($n = 1, 2, 3$) group, all the GCs are active, and their MFRs $f^{(GC)}$ increase with $M_{syn}^{(GC,EC)}$ due to increase in excitation from the EC cells. However, in the G4 and G5 groups, when $M_{syn}^{(GC,EC)}$ passes a threshold M_{th}^*, active GCs begin to appear and then their MFRs $f^{(GC)}$ also increase with $M_{syn}^{(GC,EC)}$; $M_{th}^* = 74$ and 89 for G4 and G5, respectively. In the group G6 with $M_{syn}^{(GC,HIPP)} \geqslant 7$, only silent GCs exist, independently of $M_{syn}^{(GC,EC)}$.

Figure 4(c) shows a plot of $f^{(GC)}$ (MFR of the GCs) versus $\mathcal{R}_{E-I}^{(syn)}$ (E-I synapse ratio). $\mathcal{R}_{E-I}^{(syn)}$ denotes well the competition between the excitatory EC input and the inhibitory HIPP input. We note that there exists a threshold $\mathcal{R}_{E-I}^{(syn),*}$ (=14.8), above which active GCs appear. With increasing $\mathcal{R}_{E-I}^{(syn)}$ from the threshold $\mathcal{R}_{E-I}^{(syn),*}$, MFRs $f^{(GC)}$ increase. In the active region, $f^{(GC)}$ shows a strong correlation with $\mathcal{R}_{E-I}^{(syn)}$ with the Pearson's correlation coefficient $r = 0.9389$.

B. WTA competition in the whole DG network

In this subsection, we investigate the WTA competition in the whole DG network, composed of the hilar MCs and the BCs, in addition to the EC cells, the HIPP cells, and the GCs in Fig. 3(a). Figure 5(a) shows a schematic representation in the three clusters, consisting of the excitatory GC, the inhibitory BC, and the MC. In each cluster, a GC-BC feedback loop is formed. BC receives excitation from all the GCs in the same cluster, and it provides feedback inhibition to all the GCs [lamellar connection (blue line)]. However, MC in a cluster receives excitation from all the GCs in the same cluster (lamellar connection), while they project excitation to the GCs and the BCs in other clusters [cross-lamellar connection (red)]. Thus, in the whole DG network, there are three kinds of external inputs to the GCs: two types of excitatory inputs from the EC cells via random connections and the MCs via cross-lamellar connections and one kind of inhibitory inputs from the HIPP cells via random connections. In comparison to the case in Fig. 3(a), one more excitatory input from the MCs occurs through cross-lamellar connections. These MCs tend to control firing activity of the GC-BC loop in the cluster by providing the excitatory inputs to both the GCs and the BC.

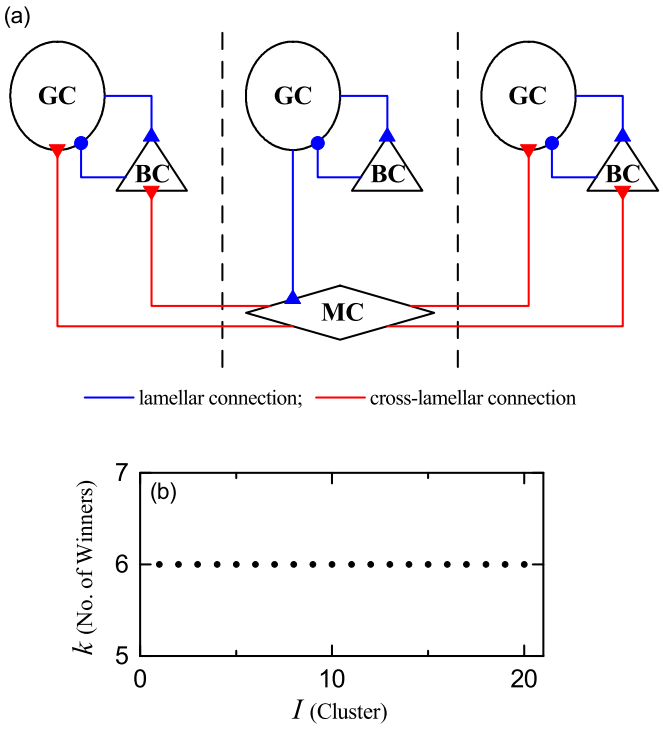

FIG. 5. WTA competition in the whole DG network. (a) Schematic representation for the three clusters, composed of the excitatory GC, the inhibitory BC, and the excitatory MC. Here, blue lines represents lamellar connections in the same clusters,while red lines denote cross-lamellar connections. (b) Plot of k (number of active GCs) versus I (cluster index).

In the whole DG network, firing activity of the GCs is determined via competition between the two excitatory EC and MC inputs and the one inhibitory HIPP input. Then, within the cluster, interaction of excitation of the GCs with feedback inhibition from the BC leads to WTA competition. Figure 5(b) shows the plot of k (number of active GCs) versus I (cluster index). Six active winner GCs appear in each cluster (i.e., $k = 6$ WTA competition occurs). Consequently, the total number of active GCs is 120, corresponding to $D_a = 6.0\,\%$ (activation degree of the GCs). In comparison to $D_a = 32.6\%$ in the presence of only the excitatory EC input and the inhibitory HIPP input (Fig. 3), sparse firing activity of the GCs results from the excitation from the MCs to the GCs and the BCs (facilitating firing activity of the GC-BC loop) and the feedback inhibition from the BC. Without the MCs, the activation degree of the GCs becomes increased to $D_a = 25.9\%$ only due to the feedback inhibitory BC input, which will be discussed in details in Fig. 9. Consequently, the MCs tend to enhance the WTA competition through facilitating firing activity of the GC-BC loop.

During the WTA competition, synchronized rhythms are found to emerge in each population of the GCs and the BCs via interaction of excitation from the GCs and inhibition from the BCs in the GC-BC loop. Figures 6(a1) and 6(a2) show raster plots of spikes of the active GCs and the BCs, respectively. We note that synchronized spiking stripes (composed of spikes and indicating population synchronization) appear successively. The corresponding IPSRs $R_{\rm GC}(t)$ and $R_{\rm BC}(t)$ exhibit synchronous oscillations with the same population frequency f_p (=13.2 Hz). In this case, the MCs control the firing activity of the GC-BC loop by providing excitation to both the GCs and the BCs via cross-lamellar connections. Thus, synchronized rhythm with f_p= 13.2 Hz is also found to appear in the population of MCs via interaction with the GCs, as shown in the raster plot of spikes and the IPSR $f_{\rm MC}(t)$ in Fig. 6(a3). Thus, in the whole DG network, synchronized rhythms with f_p= 13.2 Hz appear in the populations of the GCs, the BCs, and the MCs, together with occurrence of the WTA competition [89].

In addition to the population firing behavior, we also study the individual firing activities in terms of MFRs of active GCs, BCs, and MCs. Figures 6(b1)–6(b3) show plots of MFRs $f_i^{(\rm X)}$ of the 120 active GCs (X = GC), the 20 BCs (X = BC), and the 80 MCs (X = MC), respectively. The population-averaged MFR $\langle f_i^{(\rm X)}\rangle$ over all active cells is 2.03, 53.9, and 40.7 Hz for X = GC, BC, and MC, respectively. We note that $\langle f_i^{(\rm GC)}\rangle$ of the active GCs is much lower than $\langle f_i^{(\rm BC)}\rangle$ and $\langle f_i^{(\rm MC)}\rangle$, the reason of which is studied below.

Active GCs exhibit intermittent spikings phase-locked to the IPSR $R_{\rm GC}(t)$ at random multiples of the global period T_G (=75.8 ms) of $R_{\rm GC}(t)$. This random phase-locking results in random spike skipping, which is well shown in the inter-spike-interval (ISI) histogram with multiple peaks appearing at integer multiples of T_G in Fig. 6(c1). Spiking may occur most probably after five- and six-times spike skipping because the middle sixth- and seventh-order peaks are the highest ones, in contrast to the case of fully synchronized rhythm with only one peak at T_G (i.e., all cells fire regularly at each global cycle without skipping). In this case, the average ISI ($\langle$ISI$\rangle$) is 492.61 ms, and hence the corresponding population-averaged MFR $\langle f_i^{(\rm GC)}\rangle$ (=1 / $\langle$ISI$\rangle$ = 2.03 Hz) becomes much less than the population frequency f_p (=13.2 Hz), due to random spike skipping [89].

In contrast to the GCs, both BCs and MCs exhibit "intrastripe burstings" (corresponding to repeatedly firing bursts of spikes) within stripes, along with random spike skipping [89]. Hence, each ISI histogram becomes composed of the dominant bursting peak and the multiple random-spike-skipping peaks, as shown in Figs. 6(c2) and 6(c3); 2 (3) random-spike-skipping peaks appear for the BCs (MCs). In this way, the structure of the ISI histograms for the BCs and the MCs is distinctly different from that for the GCs, because of the occurrence of intrastripe burstings. As a result, for the BCs (MCs), the average ISI ($\langle$ISI$\rangle$) is 18.55 (24.57) ms, and hence the population-averaged MFR $\langle f_i^{(\rm BC)}\rangle$ ($\langle f_i^{(\rm MC)}\rangle$) (=1 / $\langle$ISI$\rangle$) is 53.9 (40.7) Hz, which is much higher than the population frequency f_p (=13.2 Hz) due to intrastripe burstings, in contrast to the case of the GCs with $\langle f_i^{(\rm GC)}\rangle$ (=2.03 Hz) (much lower than f_p).

From now on, we make an intensive investigation on the $k = 6$ WTA competition [shown in Fig. 5(b)] in the 1st ($I = 1$) cluster. Firing activity of the GCs is determined via competition between the external excitatory and inhibitory inputs into the GCs. Then, feedback inhibition from the BC selects which GCs fire. Only strongly active GCs may survive under the feedback inhibition. Figure 7(a) shows the plot of $f^{(\rm GC)}$ (MFR of the GCs) versus $\mathcal{R}_{\rm E-I}^{(\rm syn)}$ [E-I synapse ratio in

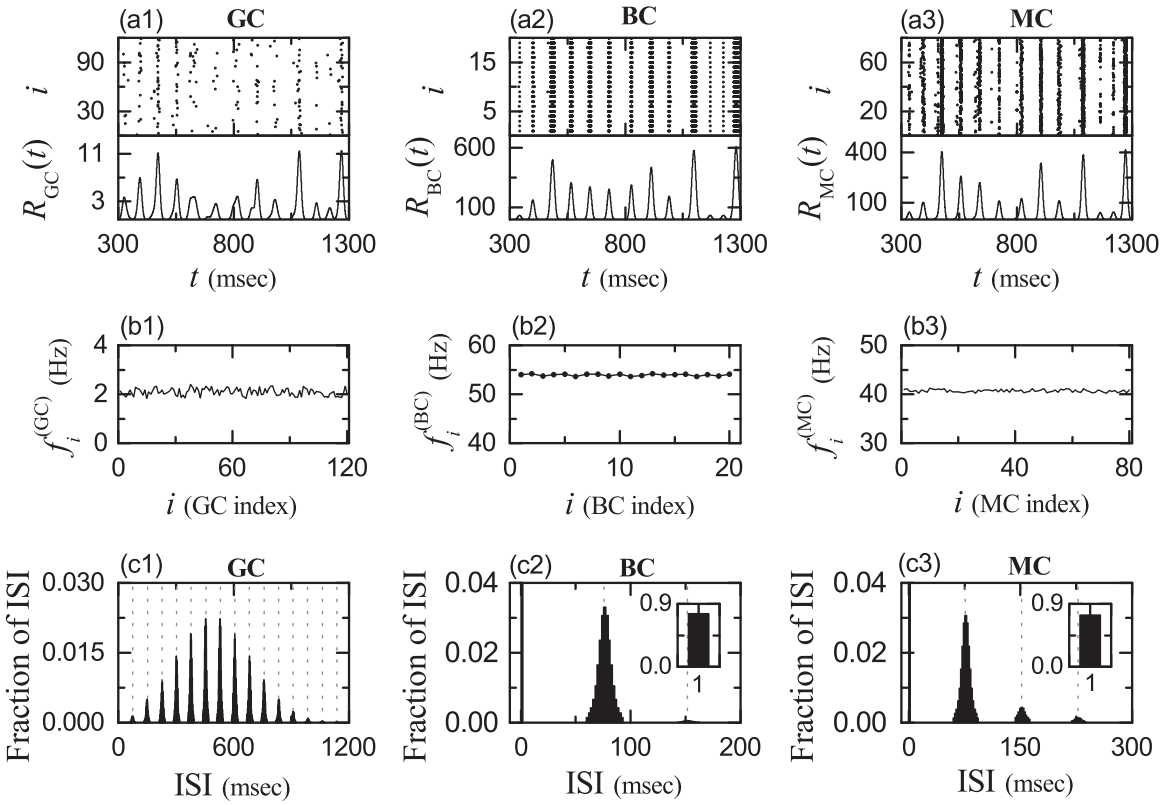

FIG. 6. Emergence of synchronized rhythms of GCs, BCs, and MCs. Raster plots of spikes and instantaneous population spike rates (IPSRs) of (a1) 120 active GCs, (a2) 20 BCs, and (a3) 80 MCs. Plots of mean firing rates (MFRs) $f_i^{(X)}$ of (b1) 120 active GCs (X = GC), (b2) 20 BCs (X = BC), and (b3) 80 MCs (X = MC). Population-averaged inter-spike-interval (ISI) histograms of (c1) 120 active GCs, (c2) 20 BCs, and (c3) 80 MCs. Vertical dotted lines in the ISI histograms represent the integer multiples of global period T_G (=75.8 ms) of the IPSR. Insets for bursting peaks are given in panels (c2) and (c3).

Eq. (1)]. There are 34 active GCs in the presence of only the external excitatory EC cells and inhibitory HIPP cells [shown in Fig. 3(a)]; for details, refer to the caption of Fig. 7(a). Among the 34 active GCs, only 6 GCs [j (GC index)= 43, 23, 36, 4, 83, and 51 with the top six highest $\mathcal{R}_{E-I}^{(syn)}$] in the G1 group (denoted by solid red circles) persist under the feedback inhibition from the BCs in the whole DG network (containing the MCs and the BCs) [shown in Fig. 5(a)], and they become winner GCs (denoted by red crosses); all the other 28 GCs with lower $\mathcal{R}_{E-I}^{(syn)}$ become silent. Figure 7(b) shows the raster plot of spikes of the 6 winner GCs in the first ($I = 1$) cluster.

We investigate the dynamical origin of the $k = 6$ WTA competition in the $I = 1$ cluster. WTA competition occurs via competition between the firing activity of the GCs and the feedback inhibition from the BC. Then, only strongly active GCs may survive under the feedback inhibition. In this case, the firing activity of the GCs is determined through competition between the external excitatory inputs from the EC cells and the MCs and the external inhibitory input from the HIPP cells. When the magnitude of the external excitatory synaptic currents is sufficiently larger than that of the external inhibitory synaptic current, the firing activity of the GCs becomes strong.

As in Eq. (B2) in Appendix B, synaptic current is given by the product of synaptic conductance g and potential difference. In this case, synaptic conductance determines the time course of the synaptic current. Hence, it is sufficient to consider the time-course of synaptic conductance. The synaptic conductance g is given by the product of synaptic strength per synapse (K), the number of synapses (M_{syn}), and the fraction s of open (postsynaptic) ion channels [see Eq. (B3)].

As in Eq. (B4), time course of $s(t)$ is given by the summation for double-exponential functions over presynaptic spikes. Here, we make an approximation of the fraction $s(t)$ of open ion channels (i.e., contributions of summed effects of presynaptic spikes) by the bin-averaged spike rate $f_X^{(I,j)}(t)$ of presynaptic neurons in the X population innervating the (I, j) GC (i.e., jth GC in the Ith cluster), as in our prior studies in the cerebellum [71,72]. Then, the excitatory conductance $g_{EC}^{(I,j)}$ for the synaptic current $I_{syn}^{(I,j)}$ from the presynaptic EC cells into the (I, j) GC is given by

$$g_{EC}^{(I,j)}(t) = g_{EC,AMPA}^{(I,j)}(t) + g_{EC,NMDA}^{(I,j)}(t) \simeq \left(K_{AMPA}^{(GC,EC)} + K_{NMDA}^{(GC,EC)}\right) M_{syn}^{(GC,EC)} f_{EC}^{(I,j)}(t). \quad (2)$$

Here, the values of $K_{AMPA}^{(GC,EC)}$ and $K_{NMDA}^{(GC,EC)}$ are given in Table II and the bin-averaged spike rate $f_{EC}^{(I,j)}(t)$ of presynaptic EC cells in the ith bin is given by

$$f_{EC}^{(I,j)}(t) = \frac{N_i^{(s)}(t)}{N_{pre}^{(I,j,EC)}\,\Delta t}, \quad (3)$$

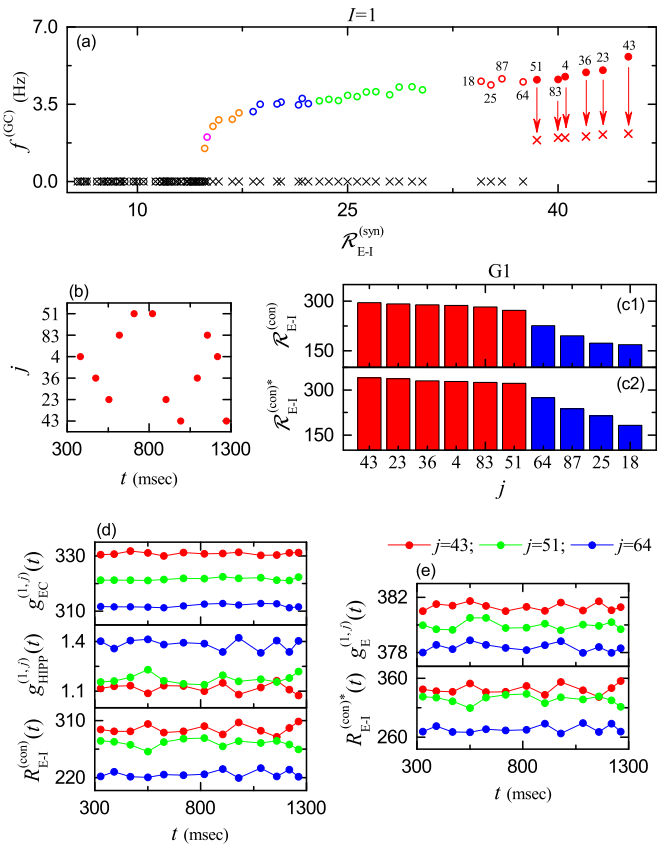

FIG. 7. Competition between the external excitatory and inhibitory inputs into the GCs, leading to $k = 6$ WTA competition. (a) Plot of $f^{(GC)}$ (MFRs of GCs) versus $\mathcal{R}^{(syn)}_{E-I}$ [$= M^{(GC,EC)}_{syn}/M^{(GC,HIPP)}_{syn}$: E-I synapse ratio in Eq. (1)] in the 1st ($I = 1$) cluster. There are 34 active GCs (denoted by circles) [10 GCs in G1 group (red), 11 GCs in G2 group (green), 7 GCs in G3 group (blue), 5 GCs in G4 group (orange), and 1 GC in G5 group (violet)] in the presence of only the external excitatory EC cells and inhibitory HIPP cells. Among the 34 active GCs, only 6 GCs in the G1 group (represented by solid red circles) persist under the feedback inhibition from the BCs in the whole DG network (including the MCs and the BCs), and they become winner GCs (represented by red crosses). (b) Raster plot of spikes of the 6 winner GCs in the 1st ($I = 1$) cluster. Plots of (c1) $\mathcal{R}^{(con)}_{E-I}$ [E-I conductance ratio of Eq. (7) in the presence of only the external excitatory EC cells and inhibitory HIPP cells] and (c2) $\mathcal{R}^{(con)*}_{E-I}$ [E-I conductance ratio of Eq. (11) in the whole network] of the 10 GCs in the 1st $G1$ group in the 1st ($I = 1$) cluster; j (x-axis label) represents GC index. Among the 10 GCs, 6 winner GCs are represented in red color, while the remaining 4 silent GCs are denoted in blue color. (d) Time courses of $g^{(1,j)}_{EC}(t)$, $g^{(1,j)}_{HIPP}(t)$, and $R^{(con)}_{E-I}(t)$ of two winner GCs [$j = 43$ (red) and $j = 51$ (green)] and one silent GC [$j = 64$ (blue)] in the 1st ($I = 1$) cluster. (e) Time courses of $g^{(1,j)}_{E}(t)$ [$= g^{(1,j)}_{EC}(t) + g^{(1,j)}_{MC}(t)$] and $\mathcal{R}^{(con)*}_{E-I}(t)$ of the two winner GCs [$j = 43$ (red) and 51 (green)] and one silent GC [$j = 64$ (blue)] in the first ($I = 1$) cluster.

where $N^{(s)}_i(t)$ is the number of spikes of the presynaptic EC cells in the ith bin, $N^{(I,j,EC)}_{pre}$ is the number of the presynaptic EC cells innervating the (I, j) GC neuron, and Δt (=75.8 ms) is the bin size. Thus, we obtain the excitatory conductance $g^{(I,j)}_{EC}$:

$$g^{(I,j)}_{EC}(t) \simeq 1.04\, M^{(GC,EC)}_{syn} f^{(I,j)}_{EC}(t). \tag{4}$$

Similarly, we also get the inhibitory conductance $g^{(I,j)}_{HIPP}$ for the synaptic current $I^{(I,j)}_{syn}$ from the presynaptic HIPP cells into the (I, j) GC:

$$g^{(I,j)}_{HIPP}(t) = g^{(I,j)}_{HIPP,GABA}(t) \simeq 0.12\, M^{(GC,HIPP)}_{syn} f^{(I,j)}_{HIPP}(t). \tag{5}$$

In Figs. 4 and 7(a), we consider only M_{syn} (number of synapses) as a "simplified" version of the synaptic input. In contrast, we now consider the "full" version of the synaptic conductance g by taking into consideration additional synaptic strength K and bin-averaged spike rate f together with M_{syn}. Then, the ratio of the external excitatory to inhibitory conductance is given by

$$R^{(con)}_{E-I}(t) = \frac{g^{(I,j)}_{EC}(t)}{g^{(I,j)}_{HIPP}(t)}. \tag{6}$$

In this case, we introduce the E-I conductance ratio $\mathcal{R}^{(con)}_{E-I}$, defined by the time average of $R^{(con)}_{E-I}(t)$:

$$\mathcal{R}^{(con)}_{E-I} = \overline{R^{(con)}_{E-I}(t)} = \overline{\frac{g^{(I,j)}_{EC}(t)}{g^{(I,j)}_{HIPP}(t)}}, \tag{7}$$

where the overline denotes time average.

The E-I conductance ratio $\mathcal{R}^{(con)}_{E-I}$, representing the time-averaged ratio of the excitatory EC to the inhibitory HIPP conductances, corresponds to a refined version in comparison to the E-I synapse ratio $\mathcal{R}^{(syn)}_{E-I}$ in Eq. (1). Figure 7(c1) shows the histogram of the E-I conductance ratio $\mathcal{R}^{(con)}_{E-I}$ versus the 10 GCs in the G1 group [denoted by red circles with GC indices in Fig. 7(a)] in the $I = 1$ cluster; 6 active GCs and 4 silent GCs are represented in red and blue color, respectively. We note that the order of magnitude of $\mathcal{R}^{(con)}_{E-I}$ is the same as that for $\mathcal{R}^{(syn)}_{E-I}$.

We next include the external excitatory MC input whose conductance is given by

$$\begin{aligned} g^{(I,j)}_{MC}(t) &= g^{(I,j)}_{MC,AMPA}(t) + g^{(I,j)}_{MC,NMDA}(t) \\ &\simeq 0.06\, M^{(GC,MC)}_{syn} f^{(I,j)}_{MC}(t). \end{aligned} \tag{8}$$

Then, we get the total excitatory input $g^{(I,j)}_{E}(t)$ via adding $g^{(I,j)}_{EC}(t)$ and $g^{(I,j)}_{MC}(t)$:

$$g^{(I,j)}_{E}(t) = g^{(I,j)}_{EC}(t) + g^{(I,j)}_{MC}(t). \tag{9}$$

In this case, the ratio of the total external excitatory to inhibitory conductance is given by

$$R^{(con)*}_{E-I}(t) = \frac{g^{(I,j)}_{E}(t)}{g^{(I,j)}_{HIPP}(t)}. \tag{10}$$

Then, in the whole network (including the MCs), we introduce the E-I conductance ratio $\mathcal{R}^{(con)*}_{E-I}$, given by the time average of $R^{(con)*}_{E-I}(t)$:

$$\mathcal{R}^{(con)*}_{E-I} = \overline{R^{(con)*}_{E-I}(t)} = \overline{\frac{g^{(I,j)}_{E}(t)}{g^{(I,j)}_{HIPP}(t)}}. \tag{11}$$

The E-I conductance ratio $\mathcal{R}_{\rm E-I}^{(\rm con)*}$ (considering the MC effect) represents the ratio of the external excitatory to the inhibitory inputs better than the E-I conductance ratio $\mathcal{R}_{\rm E-I}^{(\rm con)}$ (in the presence of only the excitatory EC and the inhibitory HIPP inputs). Hence, $\mathcal{R}_{\rm E-I}^{(\rm con)*}$ becomes a more refined version in comparison to $\mathcal{R}_{\rm E-I}^{(\rm con)}$ (which does not consider the effect of the MCs).

Figure 7(c2) shows the histogram of the (refined) E-I conductance ratio $\mathcal{R}_{\rm E-I}^{(\rm con)*}$ (considering the MC effect) versus the 10 GCs in the $I = 1$ cluster. The order of the magnitude of $\mathcal{R}_{\rm E-I}^{(\rm con)*}$ is the same as that of $\mathcal{R}_{\rm E-I}^{(\rm con)}$, and hence the 6 GCs, denoted in red color, ($j = 43$, 23, 36, 4, 83, and 51) continue to become the winners.

Figure 7(d) shows the time evolutions of $g_{\rm EC}^{(1,j)}(t)$, $g_{\rm HIPP}^{(1,j)}(t)$, and $R_{\rm E-I}^{(\rm con)}(t)$ for the top winner GC of $j = 43$, the last winner GC of $j = 51$, and the silent GC of $j = 64$ with the seventh highest $\mathcal{R}_{\rm E-I}^{(\rm con)*}$ in the $I = 1$ cluster. The order of magnitude of the EC excitatory conductance $g_{\rm EC}^{(1,j)}(t)$ is $j = 43 > j = 51 > j = 64$, while the order of magnitude of the HIPP inhibitory conductance $g_{\rm HIPP}^{(1,j)}(t)$ becomes reverse (i.e., $j = 43 < j = 51 < j = 64$). Consequently, the order of magnitude of the ratio $R_{\rm E-I}^{(\rm con)}(t)$ is $j = 43 > j = 51 > j = 64$.

By including the excitatory input from the MCs, we also consider the total excitatory conductance $g_{\rm E}^{(I,j)}(t)$ of Eq. (9) and the E-I conductance ratio $\mathcal{R}_{\rm E-I}^{(\rm con)*}$ (considering the MC effect) of Eq. (11). Figure 7(e) shows the time evolutions of $g_{\rm E}^{(1,j)}(t)$ and $R_{\rm E-I}^{(\rm con)*}(t)$ for for the top winner GC of $j = 43$, the last winner GC of $j = 51$, and the silent GC of $j = 64$. The order of magnitude of the total excitatory conductance $g_{\rm E}^{(1,j)}(t)$ is the same as that of $g_{\rm EC}^{(1,j)}(t)$ (i.e., $j = 43 > j = 51 > j = 64$). Hence, the order of magnitude of the ratio $R_{\rm E-I}^{(\rm con)*}(t)$ remains unchanged (i.e., $j = 43 > j = 51 > j = 64$). Consequently, the GCs (denoted in red color) with the top 6 highest $R_{\rm E-I}^{(\rm con)*}(t)$ in Fig. 7(c2) become the winner GCs in the whole DG network.

Figure 8(a) shows the plot of $f^{(\rm GC)}$ (MFRs of all the GCs) versus $\mathcal{R}_{\rm E-I}^{(\rm con)*}$ (E-I conductance ratio). We determine the threshold $\mathcal{R}_{\rm th}^{*}$ for the E-I conductance ratio $\mathcal{R}_{\rm E-I}^{(\rm con)*}$ (considering the MC effect). When $\mathcal{R}_{\rm E-I}^{(\rm con)*}$ passes a threshold $\mathcal{R}_{\rm th}^{*}$ (= 320.14), a discontinuous transition to an active state with nonzero $f^{(\rm GC)}$ occurs (i.e., active winner GCs with $f^{(\rm GC)} > 0$ appear). With increasing $\mathcal{R}_{\rm E-I}^{(\rm con)*}$ from the threshold $\mathcal{R}_{\rm th}^{*}$, MFRs $f^{(\rm GC)}$ increase monotonically. In the active region, $f^{(\rm GC)}$ exhibits a strong correlation with $\mathcal{R}_{\rm E-I}^{(\rm con)*}$ with the Pearson's correlation coefficient $r = 0.9787$. Figure 8(b) shows a plot of $\mathcal{R}_{\rm E-I}^{(\rm con)*}$ versus 120 winner GCs. The range of $\mathcal{R}_{\rm E-I}^{(\rm con)*}$ is $[\mathcal{R}_{\rm E-I}^{(\rm con)*}(\rm min), \mathcal{R}_{\rm E-I}^{(\rm con)*}(\rm max)]$; $\mathcal{R}_{\rm E-I}^{(\rm con)*}(\rm min) = 320.14$ and $\mathcal{R}_{\rm E-I}^{(\rm con)*}(\rm max) = 380.82$. Then, we get the winner threshold percentage $W_{th}\%$ (= 15.9%):

$$W_{\rm th}\% = \frac{\left[\mathcal{R}_{\rm E-I}^{(\rm con)*}(\rm max) - \mathcal{R}_{\rm E-I}^{(\rm con)*}(\rm min)\right]}{\mathcal{R}_{\rm E-I}^{(\rm con)*}(\rm max)} \times 100. \quad (12)$$

Thus, active winner GCs have their $\mathcal{R}_{\rm E-I}^{(\rm con)*}$ within $W_{\rm th}\%$ of the maximum $\mathcal{R}_{\rm E-I}^{(\rm con)*}(\rm max)$ of the GC with the strongest activity [i.e., GCs become active winners when their $\mathcal{R}_{\rm E-I}^{(\rm con)*}$ lies within $W_{\rm th}\%$ of the maximum $\mathcal{R}_{\rm E-I}^{(\rm con)*}(\rm max)$].

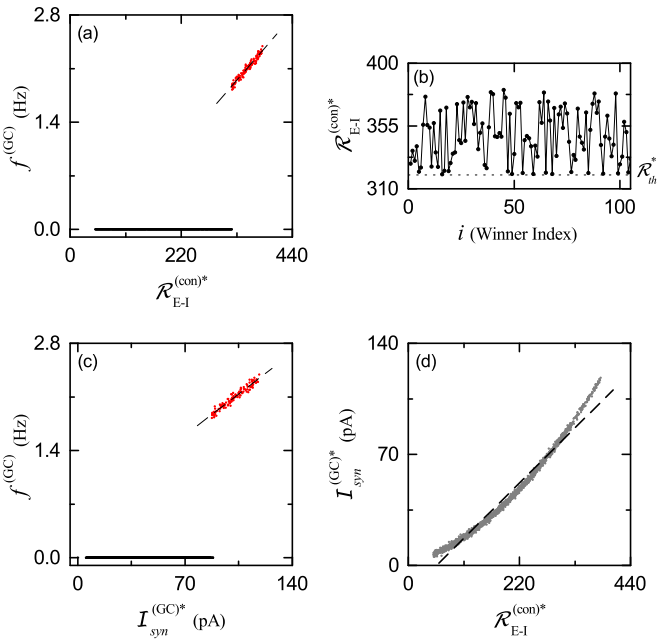

FIG. 8. Determination of the thresholds $\mathcal{R}_{\rm th}^{*}$ and $\mathcal{I}_{\rm th}^{*}$ for the winner GCs. (a) Plot of $f^{(\rm GC)}$ (MFR of all the GCs) versus $\mathcal{R}_{\rm E-I}^{(\rm con)*}$ (E-I conductance ratio which considers the effect of the MCs). (b) Plot of $\mathcal{R}_{\rm E-I}^{(\rm con)*}$ versus i (index of the 120 winner GCs). Horizontal dotted line denotes the threshold $\mathcal{R}_{\rm th}^{*}$ (= 320.14) for the winner. (c) Plot of $f^{(\rm GC)}$ versus $\mathcal{I}_{\rm syn}^{(\rm GC)*}$ [external synaptic input in Eq. (14)]. (d) Plot of $\mathcal{I}_{\rm syn}^{(\rm GC)*}$ versus $\mathcal{R}_{\rm E-I}^{(\rm con)*}$. Dashed fitted lines are given in panels (a), (c), and (d).

In addition to the external (excitatory and inhibitory) conductances, we directly consider the "external" synaptic current $I_{{\rm syn},j}^{(\rm GC,ext)}$ into the jth GC (determining the firing activity of the GC):

$$I_{{\rm syn},j}^{(\rm GC,ext)}(t) = I_{{\rm syn},j}^{(\rm GC,EC)}(t) + I_{{\rm syn},j}^{(\rm GC,HIPP)}(t) + I_{{\rm syn},j}^{(\rm GC,MC)}(t), \quad (13)$$

where $I_{{\rm syn},j}^{(\rm GC,EC)}(t)$, $I_{{\rm syn},j}^{(\rm GC,HIPP)}(t)$, and $I_{{\rm syn},j}^{(\rm GC,MC)}(t)$ are the synaptic currents into the jth GC from the EC cells, the HIPP cells, and the MCs, respectively. Then, we introduce the external synaptic input ($\mathcal{I}_{\rm syn}^{(\rm GC)*}$) into the GC, defined by the magnitude of time-average of $I_{{\rm syn},j}^{(\rm GC,ext)}(t)$:

$$\mathcal{I}_{\rm syn}^{(\rm GC)*} = \left|\overline{I_{{\rm syn},j}^{(\rm GC,ext)}(t)}\right|. \quad (14)$$

Figure 8(c) shows the plot of $f^{(\rm GC)}$ (MFRs of all the GCs) versus $\mathcal{I}_{\rm syn}^{(\rm GC)*}$. When $\mathcal{I}_{\rm syn}^{(\rm GC)*}$ passes a threshold $\mathcal{I}_{\rm th}^{*}$ (=87.3 pA), a discontinuous transition to an active state with nonzero $f^{(\rm GC)}$ takes place (i.e., active winner GCs with $f^{(\rm GC)} > 0$ emerge). As $\mathcal{I}_{\rm syn}^{(\rm GC)*}$ is increased from the threshold $\mathcal{I}_{\rm th}^{*}$, MFRs $f^{(\rm GC)}$ increase monotonically. In the active region, $f^{(\rm GC)}$ shows a strong correlation with $\mathcal{I}_{\rm syn}^{(\rm GC)*}$ with the Pearson's correlation coefficient $r = 0.9731$. We also note that the external synaptic input $\mathcal{I}_{\rm syn}^{(\rm GC)*}$ is strongly correlated with the E-I conductance ratio $\mathcal{R}_{\rm E-I}^{(\rm con)*}$ with the Pearson's correlation coefficient $r = 0.9878$, as shown in the plot of $\mathcal{I}_{\rm syn}^{(\rm GC)*}$ versus

$\mathcal{R}_{\mathrm{E-I}}^{(\mathrm{con})*}$ in Fig. 8(d). Thus, the E-I conductance ratio $\mathcal{R}_{\mathrm{E-I}}^{(\mathrm{con})*}$ would determine the external synaptic input $\mathcal{I}_{\mathrm{syn}}^{(\mathrm{GC})*}$ and the MFR $f^{(\mathrm{GC})}$.

Finally, we summarize the main results for the $k = 6$ WTA competition, obtained in this Sec. III B. We made an intensive investigation on the quantitative dynamical origin for the WTA competition. The EC and the hilar MCs are the external input sources to the GCs. Thus, there are three types of external inputs into the GCs; the direct excitatory EC input, the indirect feedforward inhibitory EC input, mediated by the HIPP cells, and the excitatory input from the MCs. Then, the firing activities of the GCs are determined through competition between the external E and I inputs to the GCs; two excitatory inputs from the EC via the PPs and from the MCs and one inhibitory input from the HIPP cells. It has been shown that the degree of the external E-I input competition may be well represented by the E-I conductance ratio $\mathcal{R}_{\mathrm{E-I}}^{(\mathrm{con})*}$ (given by the time average of the ratio of the external E to I conductances). We note that the WTA competition occurs through interaction of the firing activity of the GCs with the feedback inhibition from the BC. GCs with larger $\mathcal{R}_{\mathrm{E-I}}^{(\mathrm{con})*}$ than the threshold $\mathcal{R}_{\mathrm{th}}^{*}$ have been found to survive under the feedback inhibition, and they became winners. However, all the other GCs with smaller $\mathcal{R}_{\mathrm{E-I}}^{(\mathrm{con})*}$ became silent in response to the feedback inhibition. In this way, we have well characterized the degree of the firing activity of the GCs in terms of $\mathcal{R}_{\mathrm{E-I}}^{(\mathrm{con})*}$. Consequently, each of the 20 clusters has been found to have six GC winners (i.e., $k = 6$ WTA competition occurs in each cluster). Thus, in the whole DG network 120 active GCs became the winners among the 2000 GCs, which corresponded to the activation degree $D_a = 6.0\%$ (i.e., sparse activation).

C. Effect of the MC death on the WTA competition

We are concerned about the effect of the hilar MCs on the WTA competition. The MCs control firing activity of the GC-BC loop via monosynaptic excitation of the GCs (MC → GC) and disynaptic inhibition of the GCs, mediated by the BCs, (MC → BC → GC), as shown in Fig. 9(a). In our DG network, disynaptic strengths are stronger than monosynaptic strength (see Tables II and III). Thus, the MCs have a net inhibitory effect on the GCs via activation of the BCs [51,52]. As a result of stronger disynaptic inhibition, $k = 6$ WTA competition occurs in each cluster [see Fig. 5(b)]. However, MC loss may occur during epileptogenesis [54,55], which would be a cause of impaired pattern separation leading to memory interference. We investigate the effect of the MC death on the WTA competition through their ablation.

We first consider the case of complete MC loss. Figures 9(b1)–9(e) show the WTA competition in the DG network without the MCs. In this case, the BC activity becomes weakened, which leads to decrease in the feedback inhibition to the GCs. Then, the GC activity becomes strengthened. Thus, more winner GCs appear, as shown in Fig. 9(b1) showing the plot of k (number of winner GCs) versus I (cluster index). The range of k is [24, 28], which is much widened in comparison to the original case [see Fig. 5(b)] in the whole network with the MCs. The total number of active GCs is 518,

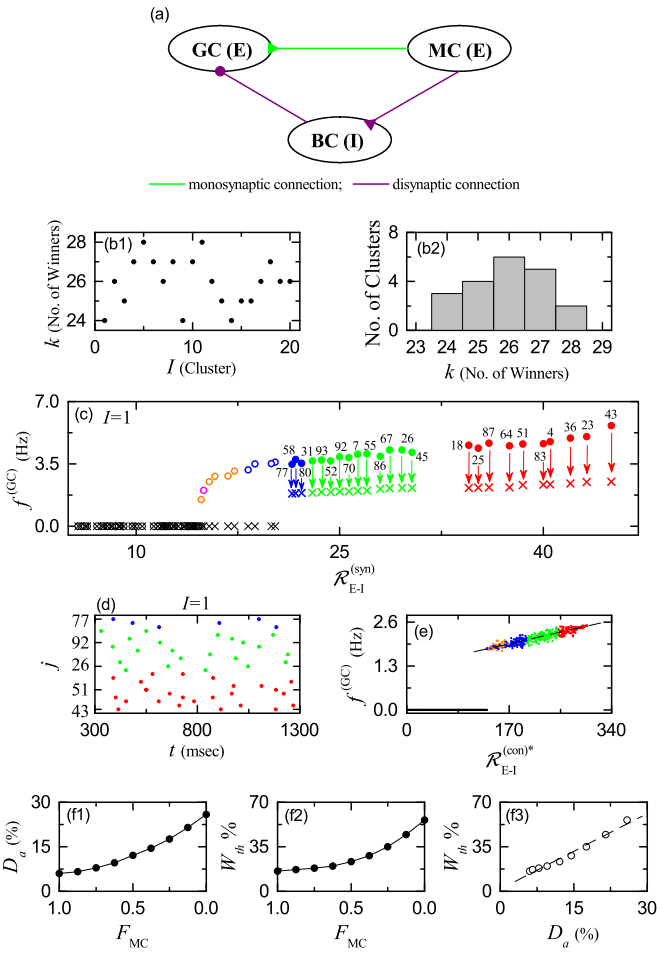

FIG. 9. Effect of MC death on the WTA competition. (a) Diagram for the monosynaptic input from the MCs (green) and the disynaptic input from the MCs, mediated by the BCs (violet) into the GCs. WTA competition in the case of F_{MC} (fraction of MCs) = 0 (i.e., complete loss of MCs) (b1–e). (b1) Plot of k (number of winner GCs) versus I (cluster index). (b2) Plot of the number of clusters versus k (number of winner GCs). First ($I = 1$) cluster in (c, d). (c) Plot of $f^{(\mathrm{GC})}$ (MFR of GCs) versus $\mathcal{R}_{\mathrm{E-I}}^{(\mathrm{syn})}$ (E-I synapse ratio). There are 34 active cells (represented by circles) in the presence of only the external excitatory EC cells and inhibitory HIPP cells); refer to Fig. 7. Among the 34 active cells, 24 GCs [10 GCs in the G1 group (red), 11 GCs in the G2 group (green), and 3 GCs in the G3 group (blue)] become winner GCs (denoted by the crosses) under the feedback inhibition of the BCs in the whole DG network. (d) Raster plot of spikes of the 24 winner GCs. (e) Plot of $f^{(\mathrm{GC})}$ (MFR of all the GCs) versus $\mathcal{R}_{\mathrm{E-I}}^{(\mathrm{con})*}$ (E-I conductance ratio); a dashed fitted line is given. (f1) Plot of D_a (activation degree) of GCs versus F_{MC} (fraction of MCs). (f2) Plot of the winner threshold percentage W_{th} % versus F_{MC}. (f3) Plot of W_{th}% versus D_a of GCs.

and hence the activation degree D_a is 25.9 %, which is much larger than $D_a = 6.0$ % in the whole network with the MCs. Figure 9(b2) also shows the plot of the number of the clusters versus k. The $k = 26$ corresponds to the most probable case where the number of the corresponding clusters is 6, and the mean value of k is also 25.9.

As an example, we consider the $I = 1$ cluster. Figure 9(c) shows the plot of $f^{(\mathrm{GC})}$ (MFR of the GCs) versus the

E-I synapse ratio $\mathcal{R}_{\mathrm{E-I}}^{(\mathrm{syn})}$. We note that 24 active winner GCs (denoted by the crosses) persist under the weakened feedback inhibition from the BC in the case of complete MC loss; for details refer to the caption of Fig. 9(c). This is in contrast to the case of the whole network (including all the MCs) in Fig. 7(a) with only 6 winner GCs. A raster plot of spikes of the 24 winner GCs is shown in Fig. 9(d).

Figure 9(e) shows the plot of $f^{(\mathrm{GC})}$ (MFR of all the GCs) versus $\mathcal{R}_{\mathrm{E-I}}^{(\mathrm{con})*}$ (E-I conductance ratio). When $\mathcal{R}_{\mathrm{E-I}}^{(\mathrm{con})*}$ passes a threshold $\mathcal{R}_{\mathrm{th}}^{*}$ (=131.22), a discontinuous transition to an active state with nonzero $f^{(\mathrm{GC})}$ occurs; 512 winner GCs with $f^{(\mathrm{GC})} > 0$ appear [156 winner GCs in the G1 group (red), 169 winner GCs in the G2 group (green), 116 winner GCs in the G3 group (blue), and 77 winner GCs in the G4 group (orange)]. The range of $\mathcal{R}_{\mathrm{E-I}}^{(\mathrm{con})*}$ for the active GCs is [131.22, 298.41]. Hence, in the case of complete loss of MCs, the winner threshold percentage $W_{\mathrm{th}}\%$ in Eq. (12) becomes 56.0 %, which is much larger than W_{th}^{*} (=15.9 %) in the whole network with MCs (see Fig. 8). Thus, active winner GCs have their $\mathcal{R}_{\mathrm{E-I}}^{(\mathrm{con})*}$ within $W_{\mathrm{th}}\%$ (=56%) of the maximum $\mathcal{R}_{\mathrm{E-I}}^{(\mathrm{con})*}(\mathrm{max})$ of the GC with the strongest activity. As a result, the WTA competition becomes so much weakened in the case of complete MC loss.

We also decrease N_{MC} (number of MCs) from 80 (in the original whole network) to 0 (complete loss). In this case, the fraction of MCs (F_{MC}) is given by $N_{\mathrm{MC}}/80$. We study the effect of MC death on the WTA competition through their ablation by varying F_{MC} from 1 to 0. The MCs provide direct excitation and indirect disynaptic inhibition (mediated by the BCs) to the GCs. In our DG network, disynaptic strengths are stronger than monosynaptic strength (i.e., the net effect of the MCs on the GCs is inhibitory [51,52]). Hence, through ablation of the MCs, their disynaptic-inhibition effect is more reduced than their monosynaptic-excitation effect, which could lead to increased activation of the GCs, supporting the dormant BC hypothesis [90,91].

Figure 9(f1) shows the plot of the activation degree D_a of the GCs versus F_{MC}. As F_{MC} is decreased from 1 to 0, the activity of the BCs becomes weakened, which results in decrease in the feedback inhibition to the GCs. Then, the activity of the GCs becomes strengthened (i.e., D_a increases monotonically from 6.0% to 25.9%), mainly due to decrease in the disynaptic-inhibition effect of the MCs. In this case, the winner threshold percentage $W_{\mathrm{th}}\%$ also increases from 15.9% to 56.0% with decreasing F_{MC} from 1 to 0, as shown in Fig. 9(f2). Due to the increased $W_{\mathrm{th}}\%$, more active GCs appear. Thus, WTA competition becomes more and more weakened with decreasing F_{MC}. Thus, the WTA competition becomes the strongest in the case of $F_{\mathrm{MC}} = 1$ where the firing activity of the GCs is the most sparse. In this way, the MCs play an important role to control the WTA competition in the GC-BC loop by providing excitation to the GCs and the BCs through cross-lamellar connections. Finally, Fig. 9(f3) shows the plot of $W_{\mathrm{th}}\%$ versus D_a. There exists a positive correlation (with the Pearson's correlation coefficient $r = 0.9889$) between $W_{\mathrm{th}}\%$ and D_a; a fitted dashed line is given. The larger the activation degree D_a of the GCs is, the higher the winner threshold percentage $W_{\mathrm{th}}\%$ becomes (i.e., the WTA competition becomes weaker).

Finally, we give a summary on the main results, obtained in this Sec. III C. We have investigated the effect of MC death on the WTA competition through their ablation by varying F_{MC} (fraction of MCs). The MCs make monosynaptic excitation of the GCs and disynaptic inhibition of the GCs, mediated by the BCs. In our DG network, disynaptic strengths are stronger than monosynaptic strength (i.e., the net effect of the MCs on the GCs is inhibitory [51,52]). Hence, through ablation of the MCs, their disynaptic-inhibition effect was more reduced than their monosynaptic-excitation effect. Consequently, with decreasing F_{MC}, both the activation degree D_a of the GCs and the winner threshold percentage $W_{\mathrm{th}}\%$ have been found to increase, and they were strongly correlated. We note that GCs become winners if their $\mathcal{R}_{\mathrm{E-I}}^{(\mathrm{con})*}$ lies within $W_{\mathrm{th}}\%$ of the maximum $\mathcal{R}_{\mathrm{E-I,max}}^{(\mathrm{con})*}$ of the GC with the strongest activity. Due to increased $W_{\mathrm{th}}\%$, the number k of the winner GCs was found to increase. Thus, with decreasing F_{MC}, the WTA competition became weakened. In this way, the hilar MCs play an important role to control the WTA competition in the GC-BC loop by providing excitation to both the GCs and the BC through cross-lamellar connections.

D. Effect of the adult-born imGCs on the WTA competition

In contrast to the MC death, adult neurogenesis occurs in the DG throughout life [16,56–61]. Thus, young imGCs appear in adulthood. In comparison to mature GCs (mGCs) (born during development), young adult-born imGCs exhibit distinct properties in physiology and connectivity such as high intrinsic excitability, low inhibition, and low excitatory innervation [56–61]. In Fig. 10(a), we consider a DG network incorporating imGCs [added in Fig. 1(a)]. For simplicity, inhibitory inputs into imGCs are neglected due to their weak sensitivity to GABAergic inhibition [56]. Figure 10(b) shows the f-I curves for the mGC (red curve) and the imGC (blue curve). The mGC with leakage reversal potential $V_L = -75$ mV (see Table I) exhibits a spiking transition when passing a threshold $I^* = 80$ mV. Here, we consider a case that the imGC has an increased leakage reversal potential $V_L = -72$ mV, which could lead to intrinsic high excitability. Then, it shows a firing transition when passing $I^* = 69.7$ pA. In this way, the imGC may have a lower firing threshold [56]. We also consider a case that the fraction of the imGCs is 10% in the whole population of GCs; the remaining 90% of the whole GCs are mGCs [16].

Similar to the case of MC death, we have studied the effect of adult-born imGCs on the WTA competition by changing the "synaptic connectivity fraction" x (corresponding to the fraction for the connection probability of the afferent excitatory synapses). In the case of mGCs, the connection probability $p^{(\mathrm{mGC,X})}$ (X = EC or MC) for the afferent excitatory synapses (EC → mGC and MC → mGC) is 20%. Due to their low synaptic connectivity, we change the connection probability $p^{(\mathrm{imGC,X})}$ for the imGCs as $20\,x$ % ($0 \leqslant x \leqslant 1$) [57]. Figure 10(c) shows plots of activation degree $D_a^{(\mathrm{X})}$ versus x (synaptic connectivity fraction) in the subpopulations of mGCs (X = m; red open circle) and imGCs (X = im; blue solid circle) and the whole population of all the GCs (X=w; green cross). Plots of the number of active GCs, $N_a^{(\mathrm{X})}$ [X = im; imGCs (solid blue circles) and X = m; mGCs (red open

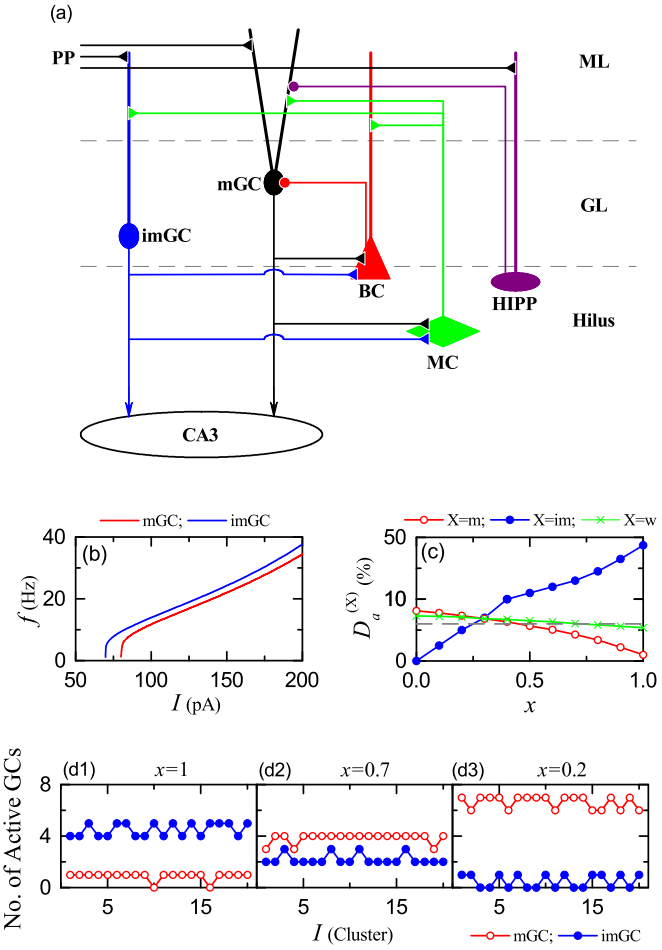

FIG. 10. Effect of adult-born immature GCs (imGCs) on the WTA competition. (a) Schematic representation of our DG network incorporating adult-born imGCs [added in Fig. 1(a)]. Fraction of the imGCs is 10% in the whole population of the GCs; fraction of mature GCs (mGCs) is 90%. Note that there are no inhibitory inputs into the imGCs, in contrast to the case of mGCs. (b) f-I curve for the mGC (red line) and the imGC (blue line). (c) Plots of activation degree $D_a^{(\mathrm{X})}$ (X = m, im, and w) versus x (synaptic connectivity fraction) in the subpopulations of mGCs (X = m) and imGCs (X = im) and in the whole population of all the GCs (X = w). Plots of number of active imGCs (blue solid circles) and mGCs (red open circles) versus I (cluster index) for x = (d1) 1, (d2) 0.75, and (d3) 0.25.

circle)] versus I (cluster) are also shown in Figs. 10(d1)–10(d3) for $x = 1.0$, 0.7 and 0.2, respectively.

For $x = 1$ [i.e., same afferent excitatory connection probability (20%) in both cases of imGCs and mGCs], imGCs exhibit very high activation degree of $D_a^{(\mathrm{im})} = 45\%$, due to their lower firing threshold, in comparison to the case of $D_a = 6\%$ without imGCs. In this case, $N_a^{(\mathrm{im})}$ (number of active imGCs) = 4 in 10 clusters and 5 in other 10 clusters [see Fig. 10(d1)]. Thus, nearly half of the 10 imGCs become active in each cluster, which results in very weakened WTA competition in the (minor) subpopulation of imGCs. These highly active imGCs in a cluster project their excitation to the BC and the MCs in the same cluster via lamellar connection. Then, the BC provides strongly increased feedback inhibition to the mGCs in the same cluster. We note that imGCs receives no feedback inhibition from the BC, and the MCs give excitation to the mGCs, imGCs, and the BCs in other clusters via cross-lamellar connections.

Thus, mGCs show sparser firing activity with much decreased activation degree $D_a^{(\mathrm{m})}$ of 1.0% due to strong feedback inhibition from the BCs. In this case, $N_a^{(\mathrm{m})}$ (number of active GCs) = 1 in 18 clusters and 0 in the remaining 2 clusters [see Fig. 10(d2)], which leads to very strengthened WTA competition in the (major) subpopulation of mGCs. In this way, the whole population of all the GCs becomes a "heterogeneous" one, composed of a (major) subpopulation of mGCs with $D_a^{(\mathrm{m})}$ of 1.0% (exhibiting strengthened WTA competition) and a (minor) subpopulation of imGCs with $D_a^{(\mathrm{im})} = 45\%$ (showing weakened WTA competition); most of active cells congregate in the minor subpopulation of imGCs. Overall in the whole population, the average activation degree $D_a^{(\mathrm{w})}$ of all the GCs becomes 5.40% (less than $D_a = 6.0\%$ in the absence of imGCs). Thus, on average, WTA competition in the whole heterogeneous population of all the GCs becomes a little strengthened, mainly due to the effect of the major subpopulation of mGCs.

In addition to the high excitability (causing high activation), we also consider the low excitatory innervation of the imGCs (leading to sparse firing), which may counteract the effect of low firing threshold [57]. As shown in Fig. 10(c), with decreasing x from 1, $D_a^{(\mathrm{im})}$ (i.e., the activation degree of imGCs; blue solid circles) decreases so rapidly (leading to increase in WTA competition); for sufficiently small x, imGCs are nearly silent. As a result, the feedback inhibition from the BC to the mGCs also becomes reduced, and hence $D_a^{(\mathrm{m})}$ (i.e., the activation degree of mGCs; red open circles) increases (resulting in decrease in WTA competition). In this way, as x is decreased, the effect of imGCs on the mGCs becomes weakened, and thus the heterogeneity degree in the whole population also becomes reduced. Due to the effect of the major mGCs, the average activation degree $D_a^{(\mathrm{w})}$ (green crosses) in the whole population also shows a slow increasing tendency (leading to slow decrease in WTA competition), and for $x < 0.4$, $D_a^{(\mathrm{w})}$ is nearly the same as $D_a^{(\mathrm{m})}$ (i.e., for $x < 0.4$, the effect of imGCs on the whole population becomes small).

As specific examples, we consider two cases of $x = 0.7$ and 0.2. For $x = 0.7$, the activation degree of the imGCs ($D_a^{(\mathrm{im})} = 22\%$) is so much decreased. As shown in Fig. 10(d2), the number of active imGCs in each cluster is decreased; $N_a^{(\mathrm{im})} = 2$ in 16 clusters and 3 in 4 clusters. In contrast, the activation degree of mGCs ($D_a^{(\mathrm{im})} = 4.28\%$) is increased. The number of active mGCs in each cluster is increased; $N_a^{(\mathrm{m})} = 3$ in 3 clusters and 4 in 17 clusters. Thus, the WTA competition is strengthened (weakened) for the imGCs (mGCs). In this case, the activation degree in the whole population ($D_a^{(\mathrm{w})} = 6.05$) becomes larger than D_a (= 6%; activation degree of the GCs without imGCs).

As x is further decreased, $D_a^{(\mathrm{im})}$ of the imGCs ($D_a^{(\mathrm{m})}$ of the mGCs) continues to decrease (increase). Eventually, they cross at $x \simeq 0.29$. For $x = 0.2$, $D_a^{(\mathrm{im})} = 5\%$, while $D_a^{(\mathrm{m})} = 7.33\%$. The imGCs exhibit sparser activation than mGCs due to very low synaptic connectivity (i.e., the imGCs show more WTA competition than the mGCs). In this case, $D_a^{(\mathrm{w})} = 7.1\%$ in the whole population of all the Gcs. Figure 10(d3) shows the number of active GCs in each cluster. For the imGCs,

$N_a^{(\mathrm{im})} = 1$ in 10 clusters and 0 in 10 clusters, while for the mGCs, $N_a^{(\mathrm{m})} = 6$ in 8 clusters and 7 in 12 clusters. In this way. for sufficiently small x, most of active cells congregate in the major subpopulation of mGCs, in contrast to the case of $x = 1$ where the minor subpopulation of imGCs has most of active cells. Thus, low excitatory innervation counteracts the effect of high excitability on the WTA competition.

Finally, we present a summary on the main results, obtained in this Sec. III D. We considered a DG network incorporating the imGCs with lower firing threshold and without receiving inhibition, and studied the effect of imGCs on the WTA competition by changing the synaptic connectivity fraction x (representing the low synaptic connectivity). When considering only the high excitability of the imGCs (i.e., $x = 1$), they became very highly active, leading to weakened WTA competition. However, mGCs (born during development) showed sparser firing activity due to strongly increased feedback inhibition from the BC (caused by the high activation of the imGCs), which resulted in strengthened WTA competition. Thus, the whole population of all the GCs became a heterogeneous one, consisting of a (major) subpopulation of mGCs (showing strengthened WTA competition) and a (minor) subpopulation of imGCs (exhibiting weakened WTA competition); most of active cells congregated in the minor subpopulation of imGCs. In addition to the high excitability (causing high activation), we also considered the low excitatory innervation of the imGCs (resulting in sparse firing), which could counteract the effect of low firing threshold [57]. With decreasing the synaptic connectivity fraction x from 1, the activation degree of imGCs $D_a^{(\mathrm{im})}$ was found to decrease so rapidly (resulting in increase in WTA competition). Consequently, the feedback inhibition from the BC to the mGCs also became reduced, and hence the activation degree of mGCs $D_a^{(\mathrm{m})}$ increased (leading to decrease in WTA competition). Thus, as x was decreased, the effect of imGCs on the mGCs became decreased (i.e., the heterogeneity degree in the whole population became reduced), and then the average activation degree of all the GCs $D_a^{(\mathrm{w})}$ in the whole population slowly increased (resulting in slow decrease in WTA competition) and became close to $D_a^{(\mathrm{m})}$.

IV. SUMMARY AND DISCUSSION

We considered the WTA competition leading to sparse activation of the GCs in a spiking neural network of the hippocampal DG. Such sparsity has been known to improve the pattern separation (preprocessed in the DG) to facilitate the pattern storage and retrieval in the CA3 [11–19]. In each lamellar cluster, a dynamical GC-BC loop is formed; all the excitatory GCs are mutually coupled with the single inhibitory BC via lamellar connections. Active GC winners are selected via competition between the firing activity of the GCs and the feedback inhibition from the BC. Intuitively, only strongly active GCs may survive under the feedback inhibition from the BC (i.e., they become winners). Through intensive computational work for WTA competition, we got the quantitative dynamical origin for the WTA competition, consistent with the intuitive thinking. Firing activities of the GCs are determined via competition between the external E and I inputs. To represent the degree of such external E-I input competition, we introduced the E-I conductance ratio $\mathcal{R}_{\mathrm{E-I}}^{(\mathrm{con})*}$ (given by the time average of the ratio of the external E to I conductances). Only the GCs with larger $\mathcal{R}_{\mathrm{E-I}}^{(\mathrm{con})*}$ than a threshold $\mathcal{R}_{\mathrm{th}}^{*}$ have thus been found to survive under the feedback inhibition from the BC, and they became winners. However, all the other GCs with smaller $\mathcal{R}_{\mathrm{E-I}}^{(\mathrm{con})*}$ became silent in response to the feedback inhibition. In this way, we have well characterized the degree of the firing activity of the GCs in terms of $\mathcal{R}_{\mathrm{E-I}}^{(\mathrm{con})*}$. Consequently, in the whole DG network 120 active GCs became the winners among the 2000 GCs, corresponding to the activation degree $D_a = 6.0\%$ (i.e., sparse activation via $k = 6$ WTA competition).

Particularly, we focused on the effect of the hilar MCs on the WTA competition. We note that the MCs control firing activity of the GC-BC loop via monosynaptic excitation of the GCs and disynaptic inhibition of the GCs, mediated by the BCs. In our DG network, disynaptic strengths are stronger than monosynaptic strength. Thus, the MCs have a net inhibitory effect on the GCs via activation of the BCs. First, we considered the effect of MC loss which may occur during epileptogenesis [54,55]. We have investigated the effect of MC death on the WTA competition through their ablation by varying F_{MC} (fraction of MCs). As F_{MC} was decreased, the activation degree D_a of the GCs has been found to increase (i.e., the number k of the winner GCs was found to increase), because the disynaptic-inhibition effect of the MCs was reduced. Consequently, with decreasing F_{MC}, the WTA competition became weakened. In contrast to MC death, young imGCs appear via adult neurogenesis [16,56–61]. We note that, the adult-born imGCs have marked properties in physiology and connectivity such as high intrinsic excitability, weak inhibition, and low excitatory innervation. We considered these distinct properties of the imGCs, and investigated their effect on the WTA competition. When considering the high excitability of imGCs, the imGCs became very highly active, while mGCs (born during development) exhibited very sparse firing activity because of strongly increased feedback inhibition from the BCs (caused by the high activation of the imGCs). Thus, the whole population of all the GCs became a very heterogeneous one, composed of a (major) subpopulation of mGCs (exhibiting strengthened WTA competition) and a (minor) subpopulation of imGCs (showing weakened WTA competition). Next, we considered the low excitatory innervation of the imGCs (resulting in sparse firing), which could counteract the effect of high excitability. As excitatory innervation of the imGCs was decreased, the activation degree of the imGCs decreased so rapidly (i.e., their WTA competition increased), while the activation degree of the mGCs increased (i.e., their WTA competition decreased). As the effect of the imGCs was decreased, the heterogeneity degree in the whole population became reduced.

Finally, we discuss limitations of our present work and future works. In our work, the degree of the firing activity of the GCs was characterized in terms of the E-I conductance ratio $\mathcal{R}_{\mathrm{E-I}}^{(\mathrm{con})*}$, and their MFRs $f^{(\mathrm{GC})}$ were found to be strongly correlated with $\mathcal{R}_{\mathrm{E-I}}^{(\mathrm{con})*}$. In addition, we directly considered the external synaptic currents into the GCs from the EC cells, the HIPP cells, and the MCs. The MFRs $f^{(\mathrm{GC})}$ were also found to be strongly associated with $\mathcal{I}_{\mathrm{syn}}^{(\mathrm{GC})*}$ (external synaptic

input, corresponding to the magnitude of time average of the external synaptic current). Obviously, $\mathcal{I}_{\rm syn}^{({\rm GC})*}$ was correlated with $\mathcal{R}_{\rm E-I}^{({\rm con})*}$. Thus, the E-I conductance ratio $\mathcal{R}_{\rm E-I}^{({\rm con})*}$ would determine the external synaptic input $I_{\rm syn}^{({\rm GC})*}$ and the MFR $f^{({\rm GC})}$. Moreover, $f^{({\rm GC})}$ was shown to exhibit a jump from 0 to a finite MFR (i.e., discontinuous transition) when passing a threshold $\mathcal{R}_{\rm th}^*$ or $\mathcal{I}_{\rm th}^*$, in contrast to the case of the single LIF neuron model with a continuous response function (i.e., continuous rectifier f-I curve). All these ones were based on computational works. For more understanding on such computational results, analytical approach would be useful. Mean-field theory has been developed for self-consistent description of population dynamics in networks of simple single neuron models (e.g., LIF neuron model), based on the probability distribution function $P(v,t)$ for the membrane potential (i.e., the probability of finding depolarization of a randomly chosen neuron at the membrane potential v and time t) [93–95]. Evolution of $P(v,t)$ may be described by the Fokker-Plank equation [96]. Thanks to the mean-field approach, the response function (i.e., population-averaged MFR versus population-averaged input) would be derived. Then, the analytic results would be expected to give some insights on our present computational results. We leave this kind of mean-field analytic approach as a future work because it is beyond the present computational work.

Here, we considered only the disynaptic inhibitory effect of the MCs on the GCs (i.e., disynaptic inhibition from the MCs to the GCs, mediated by the BC). However, we did not take into consideration the disynaptic effect of the HIPP cells on the GCs, mediated by the BCs (HIPP $\rightarrow$ BC $\rightarrow$ GC); here, we considered only their direct inhibition to the GCs (HIPP $\rightarrow$ GC). The HIPP cells may disinhibit the BC [55], and then the inhibitory effect of the BC on the GCs becomes decreased, which leads to increase in the activity of the GCs. Thus, the disynaptic effect of the HIPP cells on the GCs, mediated by the BC, tends to increase the activity of the GCs, in contrast to the disynaptic inhibition from the MCs to the GCs. Hence, in future work, to study the disynaptic effect of the HIPP cells on the GCs in the DG network would be interesting. Also, in the present work, we did not consider lamellar organization for the HIPP cells [15], the direct EC input to the MCs and the BCs [48,54], and the input from the GCs to the HIPPs [54]. For more complete network for the DG, it would be necessary to include the new lamellar organization and synaptic connections in future work.

In the present work, we studied the effect of the MCs on the WTA competition via their ablation. In this case, their disynaptic-inhibition effect was more reduced than their monosynaptic-excitation effect, and hence, with decreasing $F_{\rm MC}$ (i.e., fraction of the MCs), the activation degree D_a of the GCs was found to increase. As a future work, instead of the MC ablation, it would be interesting to investigate the WTA competition by changing the synaptic strength $K_R^{({\rm BC,MC})}$ (R = NMDA and AMPA) of the synapses from the presynaptic MCs to the postsynaptic BC. The effect of decreasing $K_R^{({\rm BC,MC})}$ would be expected to be similar to that of reducing $F_{\rm MC}$ because the synaptic inputs into the BCs are reduced in both cases.

As a future work, it would also be interesting to study the effect of imGCs on pattern separation, in addition to the effect on the WTA competition. Based on our prior work on the pattern separation [92], we just make brief discussion on the orthogonalization degree $\mathcal{O}^{({\rm X})}$ between two patterns, representing their "dissimilarity" degree, for the mGC (X = m), the imGC (X = im), and the whole GCs (X = w). This orthogonalization degree $\mathcal{O}^{({\rm X})}$ may be obtained through calculation of the Pearson's correlation coefficient $\rho^{({\rm X})}$, denoting the "similarity" degree between the two patterns; $\mathcal{O}^{({\rm X})} = (1-\rho^{({\rm X})})/2$ [92]. When the synaptic connectivity fraction x was 1 (i.e., only considering high excitability of imGCs), $\mathcal{O}^{({\rm m})}$ of the mGCs would be higher than $\mathcal{O}$ (orthogonalization degree without imGCs) because of their sparser activation degree $D_a^{({\rm m})}$ (=1.0%) (less than D_a (=6.0%) without imGCs), and hence the mGCs would perform good pattern separation [56]. However, imGCs are highly active with $D_a^{({\rm im})}$ (=45%), and hence they would be expected to have very high Pearson's correlation coefficient $\rho^{({\rm im})}$ (i.e., their orthogonalization degree $\mathcal{O}^{({\rm im})}$ would be so low), which could lead to good pattern integration (making associations between patterns). In this way, for $x = 1$ the whole population of all the GCs would be a heterogeneous one, composed of a (major) subpopulation of mGCs (good pattern separator) and a (minor) subpopulation of imGCs (good pattern integrator) [58–61]. Due to the effect of imGCs, $\mathcal{O}^{({\rm w})}$ in the whole population would be less than $\mathcal{O}$ (orthogonalization degree without imGCs).

We next consider the effect of low excitatory innervation of imGCs. With decreasing the synaptic connectivity fraction x from 1, $D_a^{({\rm im})}$ of the imGCs decreases rapidly (i.e., their firing activity becomes sparser), and hence their effect on the mGCs becomes reduced (i.e., the heterogeneity degree in the whole population is decreased). Then, $\mathcal{O}^{({\rm m})}$ of the mGCs would slowly decrease due to their increased activation degree $D_a^{({\rm m})}$ (resulting from decreased feedback inhibition). However, $\mathcal{O}^{({\rm w})}$ in the whole population would increase and approach $\mathcal{O}^{({\rm m})}$, due to decreased effect of imGCs. In this way, low excitatory innervation of imGCs could counteract the effect of high excitability [57]. For clearer understanding, more intensive work on the effect of imGCs on pattern separation is necessary, which is left as a future work because it is beyond the present work of WTA.

ACKNOWLEDGMENTS

This research was supported by the Basic Science Research Program through the National Research Foundation of Korea [NRF (KR)] funded by the Ministry of Education (KR) (Grant No. 20162007688).

APPENDIX A: LEAKY INTEGRATE-AND-FIRE SPIKING NEURON MODELS

As elements of our DG spiking neural network, we choose LIF spiking neuron models with additional AHP currents (determining the refractory period), as in our prior studies in the cerebellum [71,72]. The following equations govern evolution of dynamical states of individual cells in the X population:

$$C_X \frac{dv_i^{(X)}(t)}{dt} = -I_{L,i}^{(X)}(t) - I_{AHP,i}^{(X)}(t) + I_{\rm ext}^{(X)} - I_{{\rm syn},i}^{(X)}(t), \quad i = 1, \cdots, N_X, \tag{A1}$$

TABLE I. In the LIF spiking neuron models, parameter values for the capacitance C_X, the leaky current $I_L^{(X)}$, and the AHP current $I_{\rm AHP}^{(X)}$ of the granule cell (GC) and the basket cell (BC) in the granular layer and the mossy cell (MC) and the hilar perforant path-associated (HIPP) cell in the hilus.

		Granular layer		Hilus	
X population		GC	BC	MC	HIPP cell
C_X		106.2	232.6	206.0	94.3
$I_L^{(X)}$	$g_L^{(X)}$	3.4	23.2	5.0	2.7
	$V_L^{(X)}$	−75.0	−62.0	−62.0	−65.0
$I_{\rm AHP}^{(X)}$	$\bar{g}_{\rm AHP}^{(X)}$	10.4	76.9	78.0	52.0
	$\tau_{\rm AHP}^{(X)}$	20.0	2.0	10.0	5.0
	$V_{\rm AHP}^{(X)}$	−80.0	−75.0	−80.0	−75.0
	$v_{th}^{(X)}$	−51.5	−52.5	−32.0	−9.4

where N_X is the total number of neurons in the X population, X = GC and BC in the granular layer and X = MC and HIPP in the hilus. In Eq. (A1), C_X (pF) denotes the membrane capacitance of the cells in the X population, and the state of the ith cell in the X population at a time t (ms) is characterized by its membrane potential $v_i^{(X)}(t)$ (mV). The time evolution of $v_i^{(X)}(t)$ is governed by four types of currents (pA) into the ith cell in the X population; the leakage current $I_{L,i}^{(X)}(t)$, the AHP current $I_{{\rm AHP},i}^{(X)}(t)$, the external constant current $I_{{\rm ext},i}^{(X)}$, and the synaptic current $I_{{\rm syn},i}^{(X)}(t)$. Here, we consider a subthreshold case of $I_{\rm ext}^{(X)} = 0$ for all X [19].

In Eq. (A1), the 1st type of leakage current $I_{L,i}^{(X)}(t)$ for the ith neuron in the X population is given by

$$I_{L,i}^{(X)}(t) = g_L^{(X)}\left(v_i^{(X)}(t) - V_L^{(X)}\right), \tag{A2}$$

where $g_L^{(X)}$ and $V_L^{(X)}$ are conductance (nS) and reversal potential for the leakage current, respectively. When its membrane potential $v_i^{(X)}$ reaches a threshold $v_{\rm th}^{(X)}$ at a time $t_{f,i}^{(X)}$, the ith neuron in the X population fires a spike. After spiking (i.e., $t \geqslant t_{f,i}^{(X)}$), the second type of AHP current $I_{{\rm AHP},i}^{(X)}(t)$ follows:

$$I_{{\rm AHP},i}^{(X)}(t) = g_{\rm AHP}^{(X)}(t)\left(v_i^{(X)}(t) - V_{\rm AHP}^{(X)}\right) \quad \text{for } t \geqslant t_{f,i}^{(X)}. \tag{A3}$$

Here, $V_{\rm AHP}^{(X)}$ is the reversal potential for the AHP current, and the conductance $g_{\rm AHP}^{(X)}(t)$ is given by an exponential-decay function:

$$g_{\rm AHP}^{(X)}(t) = \bar{g}_{\rm AHP}^{(X)}\, e^{-(t-t_{f,i}^{(X)})/\tau_{\rm AHP}^{(X)}}, \tag{A4}$$

where $\bar{g}_{\rm AHP}^{(X)}$ and $\tau_{\rm AHP}^{(X)}$ are the maximum conductance and the decay time constant for the AHP current. With increasing $\tau_{\rm AHP}^{(X)}$, the refractory period becomes longer.

The parameter values for the capacitance C_X, the leakage current $I_L^{(X)}$, and the AHP current $I_{\rm AHP}^{(X)}$ of the GC, the BC, the MC, and the HIPP cell are given in Table I. These values are based on physiological properties of the GC, BC, MC, and HIPP cell [19,49].

APPENDIX B: SYNAPTIC CURRENTS

In this Appendix, we consider the fourth type of synaptic current $I_{{\rm syn},i}^{(X)}(t)$ into the ith neuron in the X population in Eq. (A1). The synaptic current $I_{{\rm syn},i}^{(X)}(t)$ consists of the following three kinds of synaptic currents:

$$I_{{\rm syn},i}^{(X)}(t) = I_{{\rm AMPA},i}^{(X,Y)}(t) + I_{{\rm NMDA},i}^{(X,Y)}(t) + I_{{\rm GABA},i}^{(X,Z)}(t). \tag{B1}$$

Here, $I_{{\rm AMPA},i}^{(X,Y)}(t)$ and $I_{{\rm NMDA},i}^{(X,Y)}(t)$ are the excitatory AMPA (α-amino-3-hydroxy-5-methyl-4-isoxazolepropionic acid) receptor-mediated and NMDA (N-methyl-D-aspartate) receptor-mediated currents from the presynaptic source Y population to the postsynaptic ith neuron in the target X population. In contrast, $I_{{\rm GABA},i}^{(X,Z)}(t)$ is the inhibitory $\rm GABA_A$ (γ-aminobutyric acid type A) receptor-mediated current from the presynaptic source Z population to the postsynaptic ith neuron in the target X population.

As in the case of the AHP current, the R (=AMPA, NMDA, or GABA) receptor-mediated synaptic current $I_{R,i}^{(T,S)}(t)$ from the presynaptic source S population to the ith postsynaptic neuron in the target T population is given by

$$I_{R,i}^{(T,S)}(t) = g_{R,i}^{(T,S)}(t)\left(v_i^{(T)}(t) - V_R^{(S)}\right), \tag{B2}$$

where $g_{(R,i)}^{(T,S)}(t)$ and $V_R^{(S)}$ are synaptic conductance and synaptic reversal potential (determined by the type of the presynaptic source S population), respectively. We obtain the synaptic conductance $g_{R,i}^{(T,S)}(t)$ from

$$g_{R,i}^{(T,S)}(t) = K_R^{(T,S)} \sum_{j=1}^{N_S} w_{ij}^{(T,S)}\, s_j^{(T,S)}(t), \tag{B3}$$

where $K_R^{(T,S)}$ is the synaptic strength per synapse for the R-mediated synaptic current from a presynaptic neuron in the source S population to a postsynaptic neuron in the target T population. The interpopulation synaptic connection from the source S population (with N_s neurons) to the target T population is given by the connection weight matrix $W^{(T,S)}$ (= $\{w_{ij}^{(T,S)}\}$) where $w_{ij}^{(T,S)} = 1$ if the jth neuron in the source S population is presynaptic to the ith neuron in the target T population; otherwise, $w_{ij}^{(T,S)} = 0$.

TABLE II. Parameters for the synaptic currents $I_R^{({\rm GC},S)}(t)$ into the GC. The GCs receive the direct excitatory input from the entorhinal cortex (EC) cells, the inhibitory input from the HIPP cells, the excitatory input from the MCs, and the feedback inhibition from the BCs.

Target cells (T)	GC					
Source cells (S)	EC cell		HIPP cell	MC		BC
Receptor (R)	AMPA	NMDA	GABA	AMPA	NMDA	GABA
$K_R^{(T,S)}$	0.89	0.15	0.12	0.05	0.01	25.0
$\tau_{R,r}^{(T,S)}$	0.1	0.33	0.9	0.1	0.33	0.9
$\tau_{R,d}^{(T,S)}$	2.5	50.0	6.8	2.5	50.0	6.8
$\tau_{R,l}^{(T,S)}$	3.0	3.0	1.6	3.0	3.0	0.85
$V_R^{(S)}$	0.0	0.0	−86.0	0.0	0.0	−86.0

TABLE III. Parameters for the synaptic currents $I_R^{(T,S)}(t)$ into the HIPP cell, MC, and BC. The HIPP cells receive the excitatory input from the EC cells, the MCs receive the excitatory input from the GCs, and the BCs receive the excitatory inputs from both the GCs and the MCs.

Target cells (T)	HIPP cell		MC		BC			
Source cells (S)	EC cell		GC		GC		MC	
Receptor (R)	AMPA	NMDA	AMPA	NMDA	AMPA	NMDA	AMPA	NMDA
$K_R^{(T,S)}$	12.0	3.04	6.84	1.22	0.38	0.02	3.23	0.19
$\tau_{R,r}^{(T,S)}$	2.0	4.8	0.5	4.0	2.5	10.0	2.5	10.0
$\tau_{R,d}^{(T,S)}$	11.0	110.0	6.2	100.0	3.5	130.0	3.5	130.0
$\tau_{R,l}^{(T,S)}$	3.0	3.0	1.5	1.5	0.8	0.8	3.0	3.0
$V_R^{(S)}$	0.0	0.0	0.0	0.0	0.0	0.0	0.0	0.0

The postsynaptic ion channels are opened due to the binding of neurotransmitters (emitted from the source S population) to receptors in the target T population. The fraction of open ion channels at time t is denoted by $s^{(T,S)}(t)$. The time course of $s_j^{(T,S)}(t)$ of the jth neuron in the source S population is given by a sum of double exponential functions $E_R^{(T,S)}(t - t_f^{(j)} - \tau_{R,l}^{(T,S)})$:

$$s_j^{(T,S)}(t) = \sum_{f=1}^{F_j^{(S)}} E_R^{(T,S)}\big(t - t_f^{(j)} - \tau_{R,l}^{(T,S)}\big), \tag{B4}$$

where $t_f^{(j)}$ and $F_j^{(S)}$ are the fth spike time and the total number of spikes of the jth neuron in the source S population, respectively. $\tau_{R,l}^{(T,S)}$ is the synaptic latency time constant for R-mediated synaptic current. The exponential-decay function $E_R^{(T,S)}(t)$ (which corresponds to contribution of a presynaptic spike occurring at $t = 0$ in the absence of synaptic latency) is given by

$$E_R^{(T,S)}(t) = \frac{1}{\tau_{R,d}^{(T,S)} - \tau_{R,r}^{(T,S)}}\big(e^{-t/\tau_{R,d}^{(T,S)}} - e^{-t/\tau_{R,r}^{(T,S)}}\big)\Theta(t), \tag{B5}$$

where $\Theta(t)$ is the Heaviside step function: $\Theta(t) = 1$ for $t \geqslant 0$ and 0 for $t < 0$. $\tau_{R,r}^{(T,S)}$ and $\tau_{R,d}^{(T,S)}$ are synaptic rising and decay time constants of the R-mediated synaptic current, respectively.

Here, Tables II and III show the parameter values for the synaptic strength per synapse $K_R^{(T,S)}$, the synaptic rising time constant $\tau_{R,r}^{(T,S)}$, synaptic decay time constant $\tau_{R,d}^{(T,S)}$, synaptic latency time constant $\tau_{R,l}^{(T,S)}$, and the synaptic reversal potential $V_R^{(S)}$ for the synaptic currents into the GCs and for the synaptic currents into the HIPP cells, the MCs and the BCs, respectively. These parameter values are also based on the physiological properties of the relevant cells [19,74–81].

APPENDIX C: INSTANTANEOUS POPULATION SPIKE RATE

Population firing activity of the active cells may be well visualized in the raster plot of spikes which is a collection of spike trains of individual active cells. In a synchronized case, synchronized spiking stripes (composed of spikes and indicating population synchronization) appear successively, while in a desynchronized case, spikes are completely scattered without forming any synchronized spiking stripes.

As a population quantity showing collective firing behaviors, we employ an instantaneous population spike rate (IPSR) which may be obtained from the raster plots of spikes [82–87]. To get a smooth IPSR, we use the kernel density estimation (kernel smoother) [97]. Each spike in the raster plot is convoluted (or blurred) with a kernel function $K_h(t)$ to get a smooth estimate of IPSR $R_{\rm EC}(t)$:

$$R_{\rm EC}(t) = \frac{1}{N_a}\sum_{i=1}^{N_a}\sum_{s=1}^{n_i} K_h\big(t - t_s^{(i)}\big), \tag{C1}$$

where N_a is the number of the active cells, $t_s^{(i)}$ is the sth spiking time of the ith active cell, n_i is the total number of spikes for the ith active cell, and we use a Gaussian kernel function of band width h:

$$K_h(t) = \frac{1}{\sqrt{2\pi}h} e^{-t^2/2h^2}, \quad -\infty < t < \infty. \tag{C2}$$

Throughout the paper, the band width h of $K_h(t)$ is 20 ms.

[1] M. A. Gluck and C. E. Myers, *Gateway to Memory: An Introduction to Neural Network Modeling of the Hippocampus in Learning and Memory* (MIT Press, Cambridge, MA, 2001).

[2] L. Squire, *Memory and Brain* (Oxford University Press, New York, NY, 1987).

[3] D. Marr, Philos. Trans. R. Soc. Lond. B **262**, 23 (1971).

[4] D. Willshaw and J. Buckingham, Philos. Trans. R. Soc., Lond. B **329**, 205 (1990).

[5] B. McNaughton and R. Morris, Trends Neurosci. **10**, 408 (1987).

[6] E. T. Rolls, Functions of neuronal networks in the hippocampus and neocortex in memory, in *Neural Models of Plasticity: Experimental and Theoretical Approaches*, edited by J. H. Byrne and W. O. Berry (Academic Press, San Diego, CA, 1989), pp. 240–265.

[7] E. T. Rolls, The representation and storage of information in neural networks in the primate cerebral cortex and

hippocampus, in *The Computing Neuron*, edited by R. Durbin, C. Miall, and G. Mitchison (Addison-Wesley, Wokingham, UK, 1989), pp. 125–159.
[8] E. T. Rolls, Functions of neuronal networks in the hippocampus and cerebral cortex in memory, in *Models of Brain Function*, edited by R. Cotterill (Cambridge University Press, New York, NY, 1989), pp. 15–33.
[9] A. Treves and E. T. Rolls, Network **2**, 371 (1991).
[10] A. Treves and E. T. Rolls, Hippocampus **2**, 189 (1992).
[11] A. Treves and E. T. Rolls, Hippocampus **4**, 374 (1994).
[12] R. C. O'Reilly and J. C. McClelland, Hippocampus **4**, 661 (1994).
[13] E. T. Rolls, Neurobiol. Learn. Mem. **129**, 4 (2016).
[14] C. E. Myers and H. E. Scharfman, Hippocampus **19**, 321 (2009).
[15] C. E. Myers and H. E. Scharfman, Hippocampus **21**, 1190 (2011).
[16] C. E. Myers, K. Bermudez-Hernandez, and H. E. Scharfman, PLoS One **8**, e68208 (2013).
[17] H. E. Scharfman and C. E. Myers, Neurobiol. Learn. Mem. **129**, 69 (2016).
[18] M. Y. Yim, A. Hanuschkin, and J. Wolfart, Hippocampus **25**, 297 (2015).
[19] S. Chavlis, P. C. Petrantonakis, and P. Poirazi, Hippocampus **27**, 89 (2017).
[20] M. A. Yassa and C. E. L. Stark, Trends Neurosci. **34**, 515 (2011).
[21] B. Schmidt, D. F. Marrone, and E. J. Markus, Behav. Brain Res. **226**, 56 (2012).
[22] J. K. Leutgeb, S. Leutgeb, M.-B. Moser, and E. I. Moser, Science **315**, 961 (2007).
[23] A. Bakker, C. B. Kirwan, M. Miller, and C. E. L. Stark, Science **319**, 1640 (2008).
[24] P. E. Gilbert, R. P. Kesner, and I. Lee, Hippocampus **11**, 626 (2001).
[25] R. P. Kesner, I. Lee, and P. Gilbert, Rev. Neurosci. **15**, 333 (2004).
[26] M. R. Hunsaker, J. S. Rosenberg, and R. P. Kesner, Hippocampus **18**, 1064 (2008).
[27] I. Lee and R. P. Kesner, Hippocampus **14**, 66 (2004).
[28] R. Coultrip, R. Granger, and G. Lynch, Neural Netw. **5**, 47 (1992).
[29] L. de Almeida, M. Idiart, and J. E. Lisman, J. Neurosci. **29**, 7497 (2009).
[30] P. C. Petrantonakis and P. Poirazi, Front. Syst. Neurosci. **8**, 141 (2014).
[31] P. C. Petrantonakis and P. Poirazi, PLoS One **10**, e0117023 (2015).
[32] C. Houghton, Behav. Brain Res. **39**, 28 (2017).
[33] C. Espinoza, S. J. Guzman, X. Zhang, and P. Jonas, Nat. Commun. **9**, 4605 (2018).
[34] L. Su, C.-J. Chang, and N. Lynch, Neural Comput. **31**, 2523 (2019).
[35] V. J. Barranca, H. Huang, and G. Kawakita, J. Comput. Neurosci. **46**, 145 (2019).
[36] N. Z. Bielczyk, K. Piskała, M. Płomecka, P. Radziński, L. Todorova, and U. Foryś, PLoS One **14**, e0211885 (2019).
[37] Y. Wang, X. Zhang, Q. Xin, W. Hung, J. Florman, J. Huo, T. Xu, Y. Xie, M. J. Alkema, M. Zhen, and Q. Wen, eLife **9**, e56942 (2020).
[38] P. Andersen, T. V. P. Bliss, and K. K. Skrede, Exp. Brain Res. **13**, 222 (1971).
[39] D. G. Amaral and M. P. Witter, Neurosci. **31**, 571 (1989).
[40] P. Andersen, A. F. Soleng, and M. Raastad, Brain Res. **886**, 165 (2000).
[41] R. S. Sloviter and T. Lømo, Front. Neural Circ. **6**, 102 (2012).
[42] P. S. Buckmaster, H. J. Wenzel, D. D. Kunkel, and P. A. Schwartzkroin, J. Comput. Neurol. **366**, 271 (1996).
[43] P. S. Buckmaster and A. L. Jongen-Rêlo, J. Neurosci. **19**, 9519 (1999).
[44] P. S. Buckmaster, R. Yamawaki, and G. F. Zhang, J. Comp. Neurol. **445**, 360 (2002).
[45] T. Nomura, T. Fukuda, Y. Aika, C. W. Heizmann, P. C. Emson, T. Kobayashi, and T. Kosaka, Brain Res. **764**, 197 (1997).
[46] T. Nomura, T. Fukuda, Y. Aika, C. W. Heizmann, P. C. Emson, T. Kobayashi, and T. Kosaka, Brain Res. **751**, 64 (1997).
[47] H. E. Scharfman and C. E. Myers, Front. Neural Circ. **6**, 106 (2013).
[48] H. E. Scharfman, Cell Tissue Res. **373**, 643 (2018).
[49] J. Lübke, M. Frotscher, and N. Spruston, J. Neurophysiol. **79**, 1518 (1998).
[50] D. G. Amaral, H. E. Scharfman, and P. Lavenex, Prog. Brain Res. **163**, 3 (2007).
[51] S. Jinde, V. Zsiros, Z. Jiang, K. Nakao, J. Pickel, K. Kohno, J. E. Belforte, and K. Nakazawa, Neuron **76**, 1189 (2012).
[52] S. Jinde, V. Zsiros, and K. Nakazawa, Front. Neural Circ. **7**, 14 (2013).
[53] A. D. H. Ratzliff, A. L. Howard, V. Santhakumar, I. Osapay, and I. Soltesz, J. Neurosci. **24**, 2259 (2004).
[54] V. Santhakumar, I. Aradi, and I. Soltesz, J. Neurophysiol. **93**, 437 (2005).
[55] R. J. Morgan, V. Santhakumar, and I. Soletsz, Prog. Brain Res. **163**, 639 (2007).
[56] A. Sahay, D. A. Wilson, and R. Hen, Neuron **70**, 582 (2011).
[57] C. V. Dieni, R. Panichi, J. B. Aimone, C. T. Kuo, J. I. Wadiche, and L. Overstreet-Wadiche, Nat. Commun. **7**, 11313 (2016).
[58] J. B. Aimone, W. Deng, and F. H. Gage, Neuron **70**, 589 (2011).
[59] J. B. Aimone and F. H. Gage, Eur. J. Neurosci. **33**, 1160 (2011).
[60] J. B. Aimone, W. Deng, and F. H. Gage, Trends Cognit. Sci. **14**, 325 (2010).
[61] J. B. Aimone, J. Wiles, and F. H. Gage, Neuron **61**, 187 (2009).
[62] H. E. Scharfman, J. Neurosci. **11**, 1660 (1991).
[63] S. Savanthrapadian, T. Meyer, C. Elgueta, S. A. Booker, I. Vida, and M. Bartos, J. Neurosci. **34**, 8197 (2014).
[64] J. A. Hosp, M. Strüber, Y. Yanagawa, K. Obata, I. Vida, P. Jonas, and M. Bartos, Hippocampus **24**, 189 (2014).
[65] T.-T. Hsu, C.-T. Lee, M.-H. Tai, and C.-C. Lien, Cerebral. Cortex **26**, 2715 (2016).
[66] Y.-C. Liu, J.-K. Cheng, and C.-C. Lien, J. Neurosci. **34**, 1344 (2014).
[67] M. J. West, L. Slomianka, and H. J. Gundersen, Anat. Rec. **231**, 482 (1991).
[68] D. G. Amaral, N. Ishizuka, and B. Claiborne, Prog. Brain Res. **83**, 1 (1990).
[69] B. L. McNaughton, C. A. Barnes, S. J. Y. Mizumori, E. J. Green, and P. E. Sharp, Contribution of granule cells to spatial representations in hippocampal circuits: A puzzle, in *Kindling and Synaptic Plasticity: The Legacy of Graham Goddar*, edited by F. Morrell (Springer-Verlag, Boston, MA, 1991), pp. 110–123.

[70] T. Hafting, M. Fyhn, S. Molden, M. B. Moser, and E. I. Moser, Nature (London) **436**, 801 (2005).
[71] S.-Y. Kim and W. Lim, Neural Netw. **134**, 173 (2021).
[72] S.-Y. Kim and W. Lim, Cognit. Neurodyn. **15**, 1067 (2021).
[73] W. Gerstner and W. Kistler, *Spiking Neuron Models* (Cambridge University Press, New York, NY, 2002).
[74] T. B. Kneisler and R. Dingledine, Hippocampus **5**, 151 (1995).
[75] J. R. P. Geiger, J. Lübke, A. Roth, M. Frotscher, and P. Jonas, Neuron **18**, 1009 (1997).
[76] M. Bartos, I. Vida, M. Frotscher, J. R. Geiger, and P. Jonas, J. Neurosci. **21**, 2687 (2001).
[77] C. Schmidt-Hieber, P. Jonas, and J. Bischofberger, J. Neurosci. **27**, 8430 (2007).
[78] P. Larimer and B. W. Strowbridge, J. Neurosci. **28**, 12212 (2008).
[79] C. Schmidt-Hieber and J. Bischofberger, J. Neurosci. **30**, 10233 (2010).
[80] R. Krueppel, S. Remy, and H. Beck, Neuron **71**, 512 (2011).
[81] P. H. Chiang, P. Y. Wu, T. W. Kuo, Y. C. Liu, C. F. Chan, T. C. Chien, J. K. Cheng, Y. Y. Huang, C.-D. Chiu, and C. C. Lien, J. Neurosci. **32**, 62 (2012).
[82] S.-Y. Kim and W. Lim, J. Neurosci. Methods **226**, 161 (2014).
[83] X.-J. Wang, Physiol. Rev. **90**, 1195 (2010).
[84] N. Brunel and X.-J. Wang, J. Neurophysiol. **90**, 415 (2003).
[85] C. Geisler, N. Brunel, and X.-J. Wang, J. Neurophysiol. **94**, 4344 (2005).
[86] N. Brunel and V. Hakim, Chaos **18**, 015113 (2008).
[87] S.-Y. Kim and W. Lim, Neural Netw. **106**, 50 (2018).
[88] K. Pearson, Proc. R. Soc. Lond. **58**, 240 (1895).
[89] S.-Y. Kim and W. Lim, Cognit. Neurodyn. (2021), https://doi.org/10.1007/s11571-021-09728-4.
[90] R. S. Sloviter, Hippocampus **1**, 41 (1991).
[91] R. S. Sloviter, Ann. Neurol. **35**, 640 (1994).
[92] S.-Y. Kim and W. Lim, Dysynaptic Effect of Hilar cells on pattern separation in a spiking neural network of hippocampal dentate gyrus (2021), bioRxiv doi: https://doi.org/10.1101/2021.09.24.461624.
[93] N. Brunel, J. Comput. Neurosci. **8**, 183 (2000).
[94] N. Brunel, Network: Comput. Neural Syst. **11**, 261 (2000).
[95] L. Hertag, D. Dustewitz, and N. Brunel, Front. Comput. Neurosci. **8**, 116 (2014).
[96] H. Risken, *Fokker–Planck Equation* (Springer, Berlin, 1989)
[97] H. Shimazaki and S. Shinomoto, J. Comput. Neurosci. **29**, 171 (2010).